

Article

Assessing Post-Monsoon Seasonal Soil Loss over Un-Gauged Stations of the Dwarkeswar and Shilabati Rivers, West Bengal, India

Ankita Mukherjee ¹, Maya Kumari ² and Varun Narayan Mishra ^{1,*} 

¹ Amity Institute of Geoinformatics and Remote Sensing (AIGIRS), Amity University, Sector 125, Noida 201313, India; mukherjeeankita535@gmail.com

² Amity School of Natural Resources & Sustainable Development (ASNRSD), Amity University, Sector 125, Noida 201313, India; mkumar10@amity.edu

* Correspondence: vnmishra@amity.edu

Abstract: This study employs the Soil and Water Assessment Tool (SWAT) model to evaluate soil loss within the Shilabati and Dwarkeswar River Basin of West Bengal, serving as a pilot investigation into soil erosion levels at ungauged stations during the post-monsoon season. Detailed data for temperature, precipitation, wind speed, solar radiation, and relative humidity for 2000–2022 were collected. A land use map, soil map, and slope map were prepared to execute the model. The model categorizes the watershed region into 19 sub-basins and 227 Hydrological Response Units (HRUs). A detailed study with regard to soil loss was carried out. A detailed examination of soil erosion patterns over four distinct time periods (2003–2007, 2007–2012, 2013–2017, and 2018–2022) indicated variability in soil loss severity across sub-basins. The years 2008–2012, characterized by lower precipitation, witnessed reduced soil erosion. Sub-basins 6, 16, 17, and 19 consistently faced substantial soil loss, while minimal erosion was observed in sub-basins 14 and 18. The absence of a definitive soil loss pattern highlights the region's susceptibility to climatic variables. Reduced soil erosion from 2018 to 2022 is attributed to diminished precipitation and subsequent lower discharge levels. The study emphasizes the intricate relationship between climatic factors and soil erosion dynamics.

Keywords: SWAT; watershed modeling; soil loss; post-monsoon season; ungauged stations; sensitivity analysis; SUFI-2



Citation: Mukherjee, A.; Kumari, M.; Mishra, V.N. Assessing Post-Monsoon Seasonal Soil Loss over Un-Gauged Stations of the Dwarkeswar and Shilabati Rivers, West Bengal, India. *Earth* **2024**, *5*, 45–71. <https://doi.org/10.3390/earth5010003>

Academic Editor: Christian Conoscenti

Received: 28 December 2023

Revised: 21 January 2024

Accepted: 1 February 2024

Published: 7 February 2024



Copyright: © 2024 by the authors. Licensee MDPI, Basel, Switzerland. This article is an open access article distributed under the terms and conditions of the Creative Commons Attribution (CC BY) license (<https://creativecommons.org/licenses/by/4.0/>).

1. Introduction

Soil, a finite resource, plays a vital role in sustaining life by serving as the foundation for food production, carbon sequestration, biodiversity enhancement, and the regulation of water and climate [1,2]. The wearing away of the topsoil layer is known as soil erosion and contributes to soil degradation. One of the biggest difficulties for land managers is land degradation, which includes soil erosion, as it affects around 60% of the world's land surface [3,4]. According to one study [5], the risk of land degradation is expected to intensify due to the dual impact of climate change and ineffective basin management. Alarming, approximately 44 percent of India is reported to be grappling with the challenge of land degradation. Because a considerable portion of the populations of developing nations directly depend on agricultural and land resources for their livelihood, the economic and social effects of soil erosion there are more severe than in industrialized countries [6–8]. Soil erosion models are helpful for planning land use plans, estimating soil loss and runoff rates from agricultural land, providing relative soil loss indices, and guiding government policy and strategy on soil and water conservation [9]. The estimated annual average rate of soil loss is roughly 16.75 t/ha, which is far higher than the 7.5 to 12.5 t/ha/yr allowed soil erosion rates for different regions of the nation [10]. In order to quantify and describe erosion in terms of parameters like the rainfall erosivity index, soil erodibility, topography,

and management techniques, among others, soil loss models often make an effort to interpret physical laws and landscape processes into mathematical correlations [11,12]. Rainfall serves as a catalyst for soil detachment and subsequent displacement, frequently involving complicated regional geomorphic processes. It contributes to soil erosion, a widespread issue that affects soil stability across the globe [13,14]. It is a major issue affecting environmental quality, agricultural productivity, and food security in many nations throughout the world [3,7,15,16]. As opposed to erosion caused by on-site deposition in micro-topographic depressions, soil loss refers to the actual amount of material taken from a particular hill slope or slope segment [12,17].

Unchecked soil loss from watersheds as a result of excessive human meddling has become a significant concern for preserving crop production sustainability and maintaining land productivity today [5,18,19]. Using various empirical and semi-empirical models, several researchers have found that GIS and remote sensing are the most trustworthy and dependable tools in the measurement of soil erosion [10,20–24]. Various models have been developed to measure soil loss with respect to the geographical conditions over an area, reflecting the regional heterogeneity of watershed parameters. These models include the Modified Universal Soil Loss Equation (MUSLE) [25], the Areal Nonpoint Source Watershed Environment Response Simulation (ANSWERS) [26], the Agricultural Nonpoint Source Pollution model (AGNPS) [27], SHETRAN [28–30], the Agricultural Catchments Research Unit (ACRU) [31], and the Soil and Water Assessment Tool (SWAT) [32]. Over decades of model development, the Soil and Water Assessment Tool (SWAT) [32,33] model has become one of the most extensively used water quality watershed- and river-basin-scale models globally [34–37] and utilized for a wide variety of hydrologic and/or environmental issues [36]. The SWAT model has gained immense popularity as it can simulate continuously for a long time and can run on a daily time step [34], providing the best results for minute changes. The model divides the entire watershed into sub-basins, which are then further subdivided into hydrological response units (HRUs), land uses, vegetation types, and soil characteristics [37,38]. This model, which explains water and sediment circulation, vegetation development, and nutrient circulation, uses daily rainfall data, maximum and minimum temperatures, solar radiation, relative air humidity, and wind speed as inputs [37,38].

Various strategies for calibration and uncertainty analysis are utilized in hydrological modeling. Effective calibration and uncertainty analysis can be accomplished using a variety of techniques, such as the multi-start (M-Simplex), general algorithm (GA), parameter solution (PARASOL), adaptive clustering covering (ACCO), SWAT Calibration Uncertainty Procedure (including PSO, PARASOL, GLUE, MCMC, and SUFI-2), and uncertainty estimation based on local error and clustering (UNEEC) [39]. SUFI-2 is the most widely used and adaptable method [38], used for parameterization, sensitivity analysis, and daily/monthly calibration and verification of hydrological parameters.

The significance of this study arises from its particular focus on the post-monsoon season in West Bengal's Shilabati and Dwarkeswar regions. During the rainy season, from June to September, we normally devote a lot of attention to monitoring soil erosion and river flow in West Bengal. However, there has been a lack of awareness of the loss of sediment in the Shilabati and Dwarkeswar River basins. These areas are vulnerable to erosion, particularly gully and rill erosion. Our research focused on the period immediately following the rainy season, from 2003 through 2022, monitoring soil loss with the help of the Soil and Water Assessment Tool (SWAT) model.

2. Study Area

The study area includes two main rivers—Shilabati River (also known as Shilai River), and Dwarkeswar River (also known as Dhalkisor) along with its tributaries, as represented in Figure 1. The Shilabati River originates in the Purulia district of West Bengal, close to the Chak Gopalpur village, passing through the districts of Bankura and Paschim Medinipur in a nearly southeast direction with a length of 26 km [40]. The main tributaries of this river

are the Joyponda, Ketia, Donai, Kubai, and Champayan rivers [40]. The undulating surfaces and plain topography with isolated lateritic soil pockets characterize the upper and lower basin areas, respectively [41,42]. The Shilabati basin is a homogeneous physical entity due to its granite gneiss geological formation, undulating plateau upland with inter-fluvial lateritic upland, eastern flowing river system, low to medium rainfall (100–140 cm), high temperature in summers (35–40 °C), and tropical dry deciduous forest cover [43]. Flooding is common in Shilabati, especially in the Banka, Khirpai, and Ghatal regions.



Figure 1. Map of (a) India showing West Bengal. (b) Study area showing the Shilabati and Dwarkeswar rivers along with their tributaries.

The Dwarkeswar River originates from the Chota Nagpur Plateau in the Purulia district, in the Panjioneya Pahar close to Tilboni Hill and moves towards the Chhatna area, dividing the area into two equal blocks in the Bankura district. It flows through the district headquarters as it cuts across the district before entering the southeast corner of East Bardhaman District and passes through Hooghly District with a length of around 113 km [40]. The tributaries of the river are Gandheshwari, Boko, Arkasha, Berai, and Shankari [40]. Before entering the Bankura district as the Kumari Nala, the other left bank tributary Danga Nala already passes the undulating surface into a web of gullies [44]. The average annual rainfall is between 140 and 150 cm [44], with seventy percent rain in the monsoon season from June to September [45], and this region also faces high temperatures from 35 to 40 °C during the summer season. In Ghatal, the Shilabati joins the Dwarkeswar and becomes known as Rupnarayan entering the Howrah District's Hooghly River close to Gadiara, which empties into the Bay of Bengal.

3. Methodology

3.1. Data Used

After the selection of the study area, Landsat 9 imagery was acquired for the year 2022 from the United States Geological Survey (USGS) Earth Explorer website for the month of March. A DEM (Digital Elevation Model) was downloaded from the Earth Data website to delineate the watershed, and a soil map was provided by the Food and

Agricultural Organization Digital Soil Map of the World (FAO-DSMW). Data for the five climatic parameters, namely, precipitation, solar radiation, relative humidity, wind, and temperature, were downloaded from the NASA Power Data website from 2000 to 2022 on a daily basis for 30 gauge stations, in and around the study area, and all necessary corrections were performed with the help of R software. Table 1 shows the list of all the data that were used for this model.

The preparation of the Land Use and Land Cover (LULC) map utilized data from Landsat and offered a comprehensive examination of the area’s land cover. Additionally, the Digital Elevation Model (DEM) (Figure A1) was derived from ASTER data to ascertain the region’s slope characteristics, while the soil map contributed insights into soil composition and its spatial distribution within the study area. A detailed discussion of these mapping efforts is presented in the results and discussion section. The amalgamation of these maps provided a detailed understanding of the region’s underlying conditions, serving as essential inputs for the SWAT model. Furthermore, the incorporation of weather parameters played a crucial role in the processing of the SWAT modeling. Figure 2 provides a detailed flowchart explaining the methodology adopted for this study.

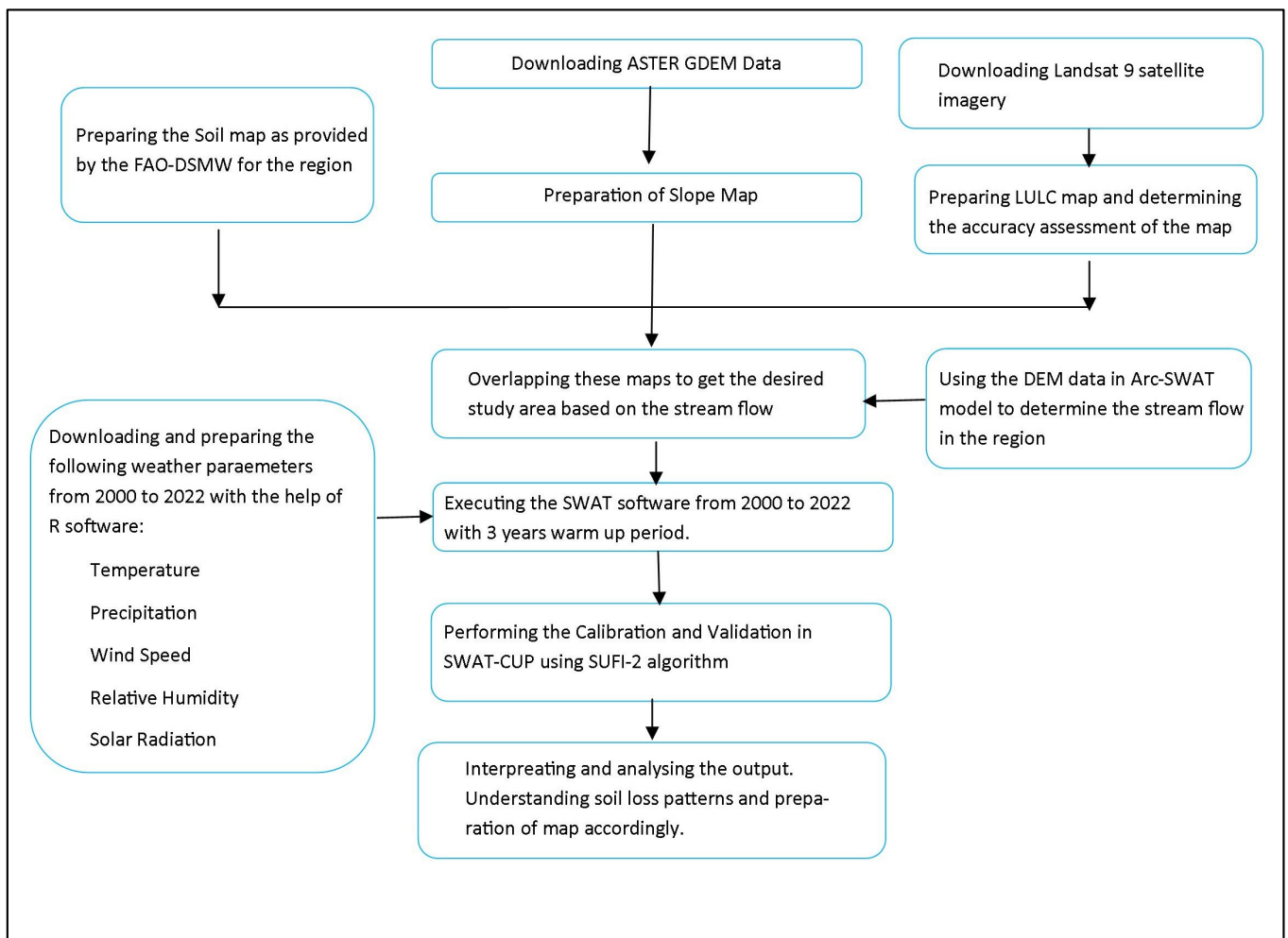


Figure 2. Methodology used.

Table 1. List of data used for the study.

Sl. No.	Data	Description	Source
1.	Digital Elevation Model (DEM)	30 m × 30 m spatial resolution grid used to delineate the boundary of the watershed.	Advanced Spaceborne Thermal Emission and Reflection Global Radiometer (ASTER) data from the United States Geological Survey (USGS)
2.	Landsat 9	To understand how the soil has been used and the current landscape; prepared by supervised classification. Resolution: 30 m × 30 m	United States Geological Survey (USGS)
3.	Soil Data	To understand the soil structure and geological structure of the watershed. Scale: 1:5,000,000	Food and Agricultural Organization Digital Soil Map of the World (FAO-DSMW)
4.	Weather	Precipitation, solar radiation, relative humidity, wind, and temperature for 30 gauge stations in and around the area from 2000 to 2022. Resolution: 0.5° × 0.625°	NASA Prediction of Worldwide Energy Resources (POWER)

3.2. Preparation of Land Use and Land Cover (LULC) Maps

Land Use and Land Cover (LULC) maps were prepared in ArcGIS with the help of a Support Vector Machine (SVM) classifier. A more precise LULC map can be obtained with the SVM classifier when compared to other supervised learning techniques [46], including maximum likelihood classification [47]. SVM is based on statistical learning theory, which is nonparametric in nature and is constructed on the basis of a small number of samples in the data found in the training text in order to achieve the best classification outcomes [47,48]. The goal of SVM is to locate a hyperplane in an N-dimensional space (where N is the number of features) that distinguishes data points into different classes. It is a classification technique for determining the optimal hyperplane that separates various classes in a dataset. SVM uses kernels if the classes are non-linearly separable. In this study, radial basis function (RBF) kernel was used, because of its ability to handle non-linear relationships between the training data and the entire dataset. RBF requires less computational time and can work effectively for non-linearly separable classes.

3.3. SWAT Setup

The Soil and Water Assessment Tool (SWAT) is a model that was created at the level of a river basin to assess the effects of land management techniques in substantial, intricate reservoirs. The hydrological model deals with the following topics: weather, a surface waterway, a return canal, a water source, soil loss, ventilation, transmission loss, pond and reservoir storage, agricultural growth and irrigation, a reaching path, nutrient and pesticide loading, and water transfers. The hydrological response unit (HRU) used by SWAT, describes local variety, which includes the properties of the soil, the land cover, and the land slope.

The equation of the SWAT model is shown in Equation (1):

$$SW_t = SW_o + \sum_{i=1}^t (R_{day} - Q_{surf} - E_a - W_{seep} - Q_{gw}) \quad (1)$$

where SW_t shows the final water content in millimeters (mm);

SW_o is the quantity of water on the first soil of the day in millimeters;

t is the number of days;

R_{day} represents the amount of precipitation on day i (mm);

Q_{surf} represents the amount of surface runoff on a given day i (mm);

E_a represents the amount of evapotranspiration on day i (mm);

W_{seep} represents the amount of water that percolated into the vadose zone from the soil profile on day i (mm);

Q_{gw} represents the amount of return flow on day i (mm).

With the help of the MUSLE provided in [9], the SWAT model forecasts soil loss. To calculate the overall fluxes from sub-basins, sediment yield is determined individually at the HRU scale using Equation (2)

$$S_y = 11.8 \left(Q_{surf} \cdot q_{peak} \cdot A_{hru} \right)^{0.56} \cdot K_{USLE} \cdot LS_{USLE} \cdot C_{USLE} \cdot P_{USLE} \cdot CFRG \quad (2)$$

where S_y is the daily sediment yield (in mg);

Q_{surf} shows the surface runoff;

q_{peak} represents the peak runoff rates;

A_{hru} is the HRU's area (in ha), K_{USLE} is the soil erodibility component;

C_{USLE} shows the surface cover and crop management factor;

P_{USLE} represents the conservation practice factor;

LS_{USLE} is the topography factor; and

$CFRG$ means the coarse fragment factor.

3.4. Model Calibration and Validation

SWAT includes a number of factors that indicate distinct hydrological conditions and traits in a watershed. During the calibration procedure, the model parameters were changed to provide outputs that were reasonably similar to the measured values. Following the model setup, auto-calibration using the SUFI-2 algorithm was performed in SWAT-CUP using the observed discharged data for the 15-year period from 2003 to 2017 at a daily time step with three years as a warm-up period (2000–2002). During the calibration process, the choice of sensitive parameters and parameter uncertainty were accessed. Utilizing calibrated values for daily discharged values, validation of the model was performed for the five-year period from 2018 to 2022. Based on the geophysical parameters of the sub-basins and the sub-basin-wise model simulated sediment yield data, watershed prioritization was carried out.

The effectiveness of the model was assessed using statistical measures such as coefficient of determination (R^2) [49] (Equation (3)), Nash–Sutcliffe Efficiency (NSE) [50] (Equation (4)), and percentage bias ($PBIAS$) [51] (Equation (5)).

$$R^2 = \frac{[\sum_{i=1}^n (S_i - \bar{S})(O_i - \bar{O})]^2}{\sum_{i=1}^n (S_i - \bar{S})^2 \cdot \sum_{i=1}^n (O_i - \bar{O})^2} \quad (3)$$

$$NSE = 1 - \frac{\sum_{i=1}^N (O_i - S_i)^2}{\sum_{i=1}^N (O_i - \bar{O})^2} \quad (4)$$

$$PBIAS = \frac{\sum_{i=1}^N (O_i - S_i)}{\sum_{i=1}^N O_i} \times 100 \quad (5)$$

where O_i is the observed data on i -th day, S_i is the model simulated value on i -th day, \bar{O} refers to the mean of observed data, \bar{S} is the average of simulated data, and N indicates the number of years of simulation. Better model performance is indicated by a higher R^2 value [52,53]. The NSE shows the statistical association between observed and simulated values from the model. Its value ranges from zero to one. According to [52,53], the model performance increases with an increase in the value of the NSE . The average tendency of simulated values, whether they are smaller or larger than their observed values, is measured using the $PBIAS$. According to [53], the appropriate value lies between -20 and $+20\%$. Positive $PBIAS$ values indicate model overestimation, whereas negative values indicate model underestimation [53]. This algorithm also calculates the P-factor and R-

factor during its calibration and validation. The fraction of observed data included within the 95% prediction border is represented by the P-factor [53]. The P-factor has a range of 0.0 to 1.0; a number close to 1.0 implies that the model is performing very well and efficiently [53,54], and a value of >0.7 or 0.75 is considered to be sufficient for discharge [54]. On the other hand, the R-factor is the ratio of the standard deviation of the measured variable to the average width of the 95PPU band. This index should have a value of 0 to less than or equal to 1.5, again depending on the circumstances [38,54,55]. Values close to 1 are acceptable for the calibration and validation of a catchment with respect to its discharge [17,54,56]. The formulas for these calculations are shown in Equations (6) and (7).

$$P - factor = ny_{ti}/N \quad (6)$$

where ny_{ti} is the number of measured values bracketed by 95PPU and N total number of observed data.

$$R - factor = \frac{\frac{1}{N} \sum_{ti=1}^n (y_{ti,97.5\%}^M - y_{ti,2.5\%}^M)}{\sigma_o} \quad (7)$$

where $y_{ti,2.5\%}^M$ and $y_{ti,97.5\%}^M$ are the lower and upper boundaries of the 95PPU band, respectively, and σ_o is the standard deviation of the observed data.

3.5. Assessment of Sediment Yield

In the course of this study, the SWAT model's output was meticulously scrutinized for the designated study area. An intricate analysis was conducted to discern the correlations among precipitation, discharge, and soil loss, shedding light on the extent of soil erosion. To gauge the magnitude of soil loss in a granular manner, calculations were performed on a sub-basin level, and maps were meticulously crafted to depict the distribution of soil loss.

4. Results and Discussion

4.1. Land Use Land Cover (LULC)

One of the most important parts of the hydrological process is the Land Use Land Cover (LULC) map, and the area has been classified into five classes. Codes such as AGRC (agriculture), BARR (barren/fallow land), FRSD (forest), WATR (water body), and URFD (settlement) have been allocated to the LULC map, as illustrated in Figure 3. The figure also includes a graphic representation stating the percentage covered by each land cover type. Agriculture is an important source of revenue, particularly in the south, although sparser agricultural zones can be found in the middle. As one moves towards the north, barren land predominates, making farming unfeasible owing to gully erosion. There are also sparse pockets of barren ground in the west, with smaller spots of thick vegetation distributed around the territory, primarily towards the center. Clustered villages are most common in the north. Due to inadequate irrigation resources, rain-fed agriculture prevails in the drought-prone Purulia district.

The LULC map exhibits an overall accuracy of 89.10%, as reflected in Table A1, along with a kappa coefficient of 0.85 (equivalent to 85% accuracy). However, the presence of mixed land use and land cover in this region poses challenges, making it more intricate to enhance the precision of the LULC results. Studies also reported that in their study that rills (26%), gullies (11%), and sheet wash (63%) were the most often seen types of erosion [57,58].

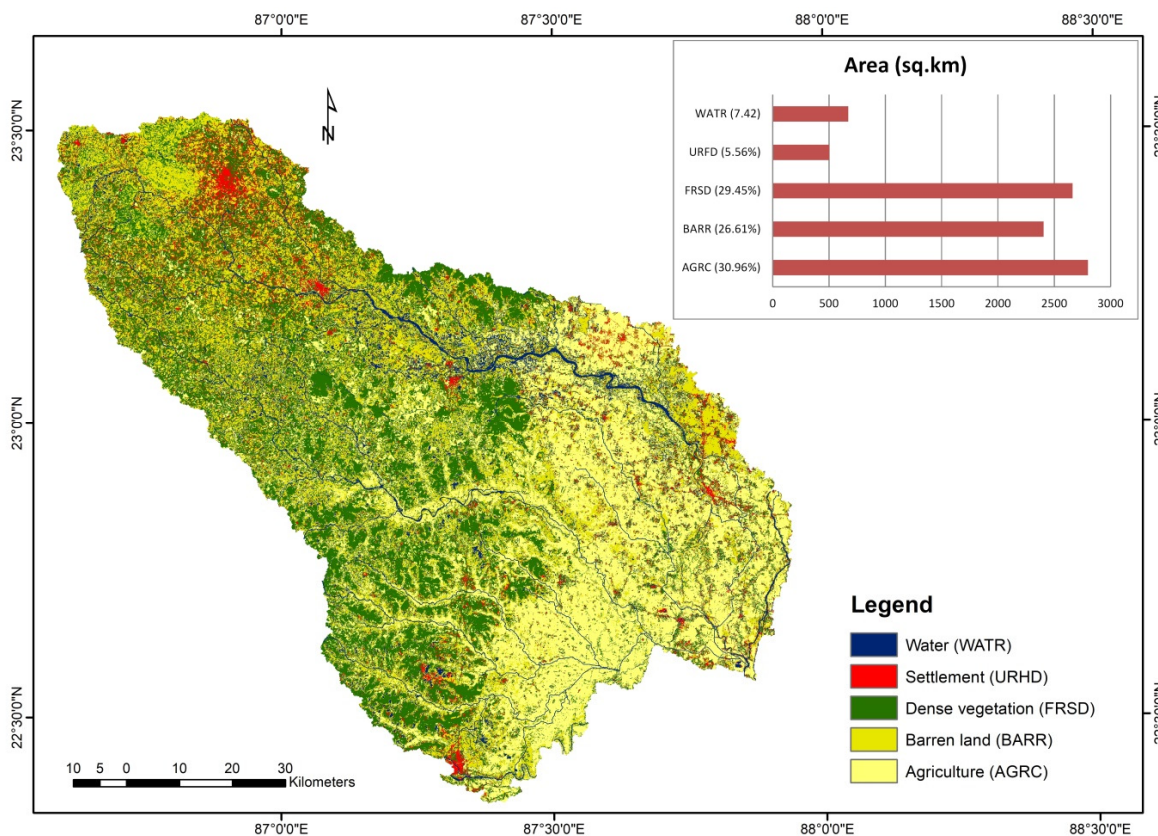


Figure 3. Land Use Land Cover Map of the study area, 2022.

4.2. Soil Map

The region is mainly divided into three major soil classes, namely, loam, sandy loam, and sandy clay loam, which are subdivided into seven different categories of soil based on their properties. The sandy loamy soil (Lf32-1b-3788) is mainly predominant in the northeastern part of the area along with sandy loam soil (Je71-2a-3758) covering a small portion while the sandy clay loam soil (Lf10-2a-6665 and Lf96-2ab-6668) is present in the central part of the area. The southwestern part of the watershed is mainly a combination of different categories of loamy soil (Be80-2a-3681, Je71-2a-3758, and Lo49-2a-3808). An area of more than 3000 km² covered by loamy soil is the best suited for agriculture, and it can be seen that agriculture is also practiced in those regions. On the other side, the sandy clay loam soil which covers more than 3500 km² is unfit for agriculture as it comprises a high proportion of sand. The sandy loam soil is the most unsuitable soil type containing the highest amount of sand, covering an area around 2360 km². If we correlate with the prepared Land Use Land Cover map, it is observed that barren land is most predominant in this soil type. Figure 4 shows the spatial distribution of soil in the area along with the percentage coverage in the area.

4.3. Slope Map

The gradient or incline of the terrain is defined as the slope. A steep slope is an abrupt incline, and a gentle slope is a gradual incline. The study region has been divided into five separate slope classes, as shown in Figure 5. The first category, with slopes ranging from 0° to 2°, is found in surrounding bodies of water, such as lakes, ponds, and rivers. It can also be found in the southwest, where agriculture is prevalent. The second category, which includes farming, barren land, and settlements, and ranges from 2° to 7°, is prevalent in the southern and southwestern regions. This slope range extends towards the northern area, where barren ground and farmland can be found. The mid-range represents dense vegetation zones, with slopes ranging from 7° to 20°. Reserve woods of note include the

Jangal Mahal, Gohaldanga Forest Range, Lalgarh-Jhitka Forest Range, Sijua Forest, Salboni Forest Range, and Badutala Reserve Forest. The remaining two categories, with slopes ranging from 20° to 35° and greater than 35°, are less common. They congregate in the northwest, near Shusunia Hill, beside villages and tourist attractions.

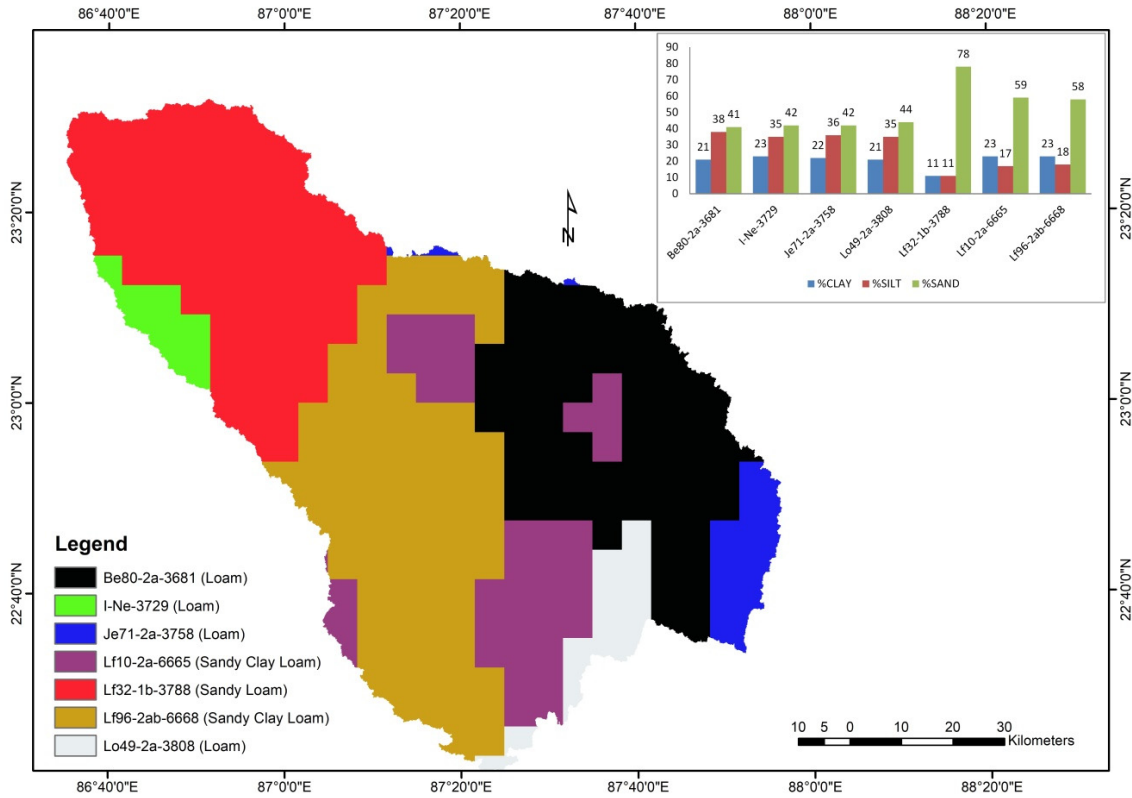


Figure 4. Soil map of the study area.

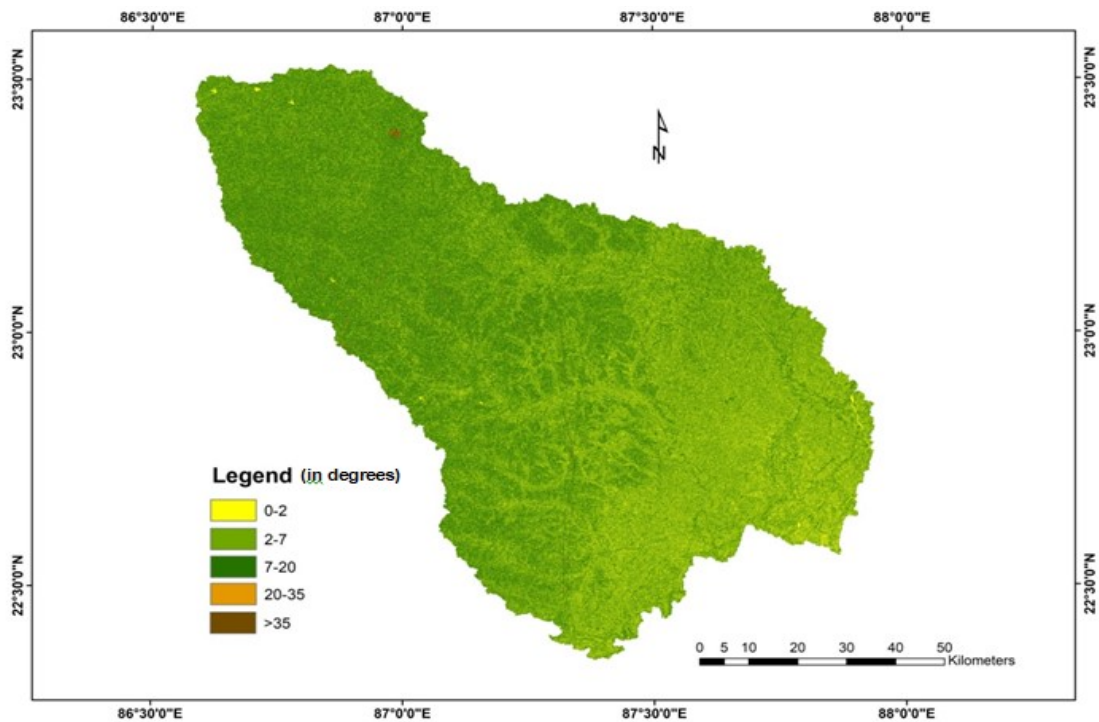


Figure 5. Slope map of the study area.

4.4. Watershed Delineation, and the Identification of Sub-Basins and HRUs

A crucial initial step in the majority of environmental and natural resource assessments, analysis, and research is the definition of watersheds and hydro-geomorphic features [59]. With the help of the Arc SWAT model, the watershed along with nineteen other sub-basins has been delimited, as represented in Figure 6. The total area of the watershed is 9039.43 km², while sub-basin 7 has the largest area of about 1023.8 km², covering almost 11.33% of the total area, followed by sub-basin 15 with 928.48 km² (10.27% of the total area). The smallest basins outlined were sub-basin 4 and sub-basin 2 with an area covering 131 km² and 181.24 km², respectively. These sub-basins have further been divided into 227 hydrological response units (HRUs) (a detailed list of HRUs is provided in Table A2) based on various soil types and land cover changes.

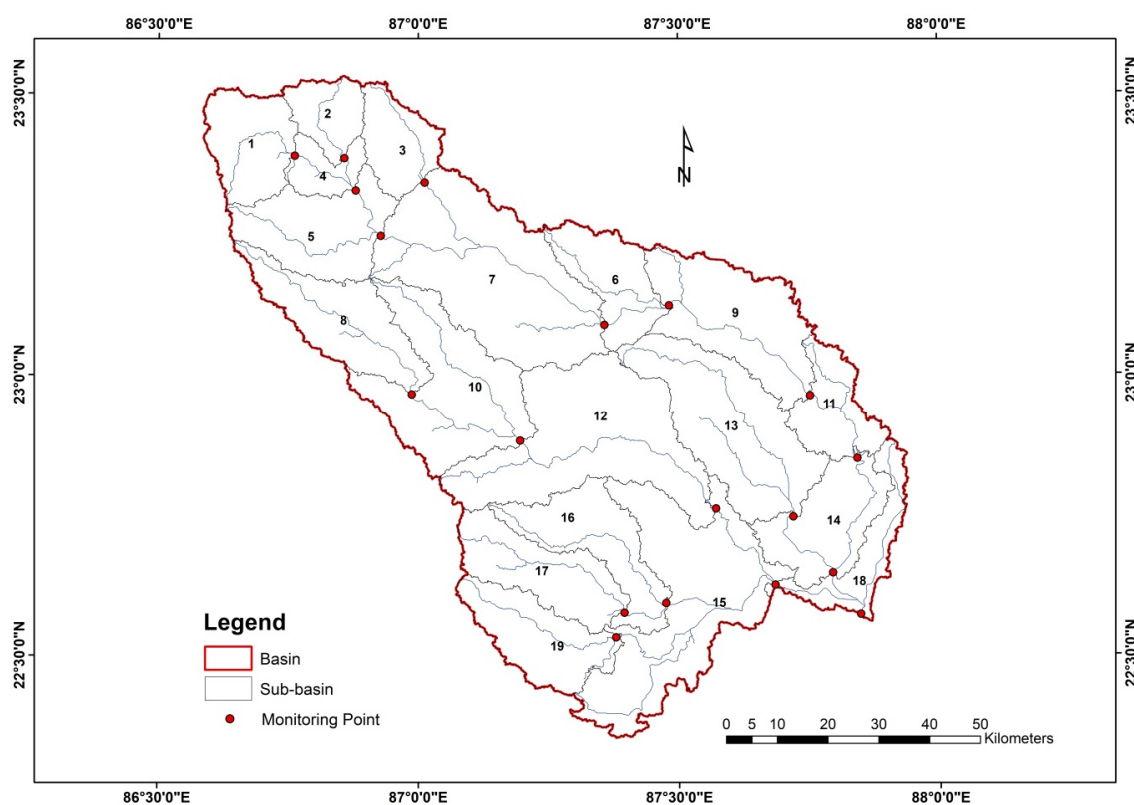


Figure 6. Watershed and sub-basin delineation of the study area.

Sub-basin 15 has the highest number of HRUs (23), followed by basin 6 with 22 HRUs and basin 12 with 19 HRUs, representing the extremely heterogeneous condition of the area. The 155th HRU in sub-basin 15 covers the maximum portion of the watershed region with 3.31%, followed by the 126th HRU in sub-basin 13 with 3.01%. The 155th HRU is located in a combination of agricultural lands, including sandy loam soil (11% clay, 11% silt, 78% sand), with a slope range from 2 to 7 degrees. Sandy loam soil is the best for cultivation in this region and supports agricultural practices in the largest HRU of the basin. It also covers 32.34% of the entire sub-basin area. The second largest HRU (126) covers 38.79% of basin 13. It is also a combination of agricultural land, along with loamy soil (21% clay, 38% silt, 41% sand) with a slope range from 2 to 7 degrees. The 155th HRU is the third largest in this region and covers an area of 3.31 in sub-basin 15. This HRU is also a combination of agricultural land, along with sandy loam soil (11% clay, 11% silt, 78% sand) with a slope range from 2 to 7 degrees. The 210th HRU covers the largest portion of any sub-basin. It covers an area of 44.72% of the 18th basin. The HRUs 43, 97, 133, 195, and 201 show the smallest area coverage of (0.02%) in the entire basin. These HRUs are mostly covered by barren land with a slope range between 0 and 2 degrees. Sub-basin 5 shows the most

homogenous type of HRU, where only four units have been identified and each unit covers more than 20% of the entire watershed, with the 22nd HRU covering the highest area of 28.48%. On the other hand, HRUs 4, 21, 22, 23, 48, 49, 55, 56, 72, 79, 104, 105, 114, 118, 142, 156, 159, 187, 210, and 213 cover an area between 1 and 2% of the total region.

4.5. Sensitivity Analysis

Due to the unavailability of sediment measuring data at the study site, our research employs runoff data for model calibration. The sensitivity analysis of runoff is conducted using the ‘Sensitivity Analysis’ function in SWAT CUP. A similar approach was also taken in [19]. By consulting the pertinent literature [52,60–63], a set of model parameters for sensitivity analysis was chosen. Following the SWAT model setup and inclusion of all input parameters, simulations and sensitivity analysis for the period 2003–2022 were performed. The findings demonstrate that the metrics that indicate surface runoff, groundwater, and soil qualities are the most vulnerable. Table 2 shows the list of parameters used, and their respective ranks. Following the outcomes of this procedure, parameters were carefully chosen for the calibration process to ensure that the evaluation coefficients meet specified criteria, ultimately achieving the highest level of accuracy in the model.

Table 2. Parameters according to their ranks used for sensitivity analysis.

Rank	Parameters	Description	Maximum Value	Minimum Value	Fitted Value
1	CN2	Curve number II	30	450	0.016
2	GW_DELAY	Groundwater delay time	0	1	53.100
3	ALPHA_BF	Base flow alpha factor	0	2	0.109
4	GWQMN	Threshold depth of water in the shallow aquifer required for return flow	0	2	0.138
5	GW_REVAP	Groundwater “revap” coefficient	0	500	0.110
6	REVAPMN	Threshold depth of water in the shallow aquifer for “revap” to occur	−0.2	0.4	312.500
7	SOL_AWC	Soil available water capacity	0.8	1	0.192
8	ESCO	Soil evaporation compensation factor	−0.8	0.8	0.942
9	SOL_K	Saturated hydraulic conductivity	0	1	−0.254
10	ALPHA_BNK	Base flow alpha factor for bank storage	5	130	0.525
11	CH_K2	Effective hydraulic conductivity in the main channel	0	1	30.875
12	EPCO	Plant uptake compensation factor	0	1	0.127
13	HRU_SLP	Average slope steepness	0	0.3	0.787
14	CH_N2	Manning’s “n” value for the main channel	0.01	1	0.104
15	OV_N	Manning’s “n” value for overland flow	−0.5	0.6	0.793
16	SLSUBBSN	Average slope length	−0.5	0.6	20.220
17	SOL_BD	Moist bulk density	0.05	24	−0.492
18	SURLAG	Surface runoff lag time	30	450	0.016

4.6. Model Calibration and Validation

Calibration is the synchronization of the model’s parameters and the uncertainty in the arbitrage margins, which results in the model’s acquisition of an interest process representation that meets predetermined requirements [64]. The calibration and validation datasets are often divided into two sets for the temporal data series. Typically, additional data from the years (between 60 and 70 percent) are used during the calibration phase. The model was calibrated for the 15-year time period from 2003 to 2017, and was validated for the remaining 5 years from 2018 to 2022 using SUFI2 for discharge data. The first 3 years

(2000 to 2022) were used as a warm-up period. Once the calibration process was completed, the new ranges of parameters were used which were generated after the calibration of the data. The model was iterated 500 times for better results, as directed in [55] and yielded outstanding results, with R^2 and NSE values of 0.99 for both calibration and validation periods. During the calibration process, the 107th simulation gave the best result, and the P-factor, R-factor, and PBIAS were 0.77, 0.89, and -0.6 , respectively, while for validation, the values were 0.92, 0.87, and -2.7 , respectively, as shown in Table 3.

Table 3. Statistical results of the model calibration and validation.

Process	R^2	NSE	P-Factor	R-Factor	PBIAS
Calibration (2003–2017)	0.95	0.97	0.77	0.89	-0.6
Validation (2018–2022)	0.92	0.93	0.98	0.87	-2.7

The 95PPU (95 percent prediction uncertainty), shown in green in Figures 7 and 8 for the calibration and validation processes, represents how SUFI2, a program in SWAT-CUP, expresses prediction uncertainty. This study’s findings indicate that during the calibration and validation phases, approximately 77% and 98% of the observed data from the donor catchment fell within the 95PPU, which represents a zone of reduced uncertainty. Similarly, the 95PPU’s narrower width (R-factors of 0.89 and 0.87 for calibration and validation) suggests that the modeling process for the donor catchment was more certain. The model also demonstrated good performance based on metrics like NSE, R^2 , and PBIAS.

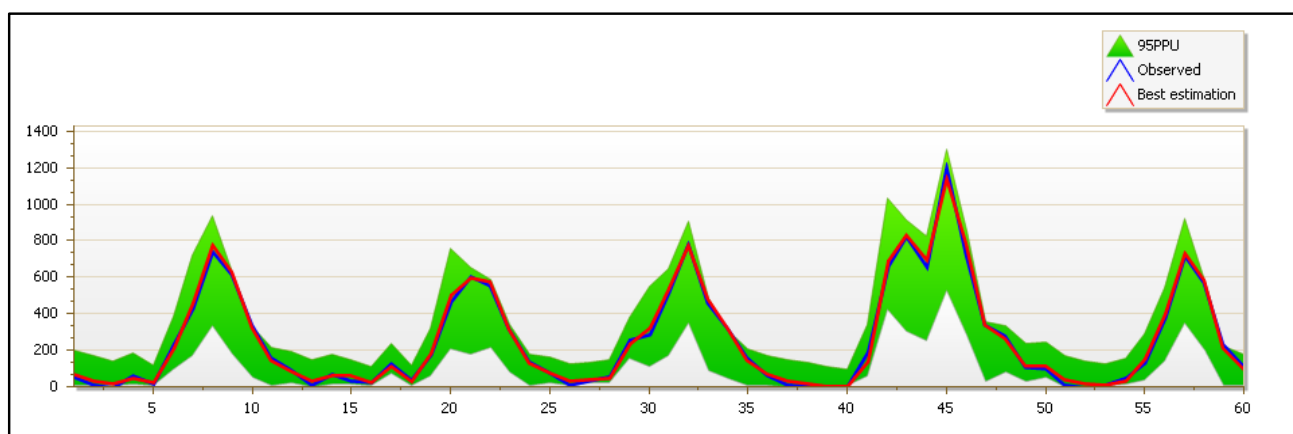


Figure 7. Comparison of measured and predicted monthly stream flow during the calibration period (2003–2017).

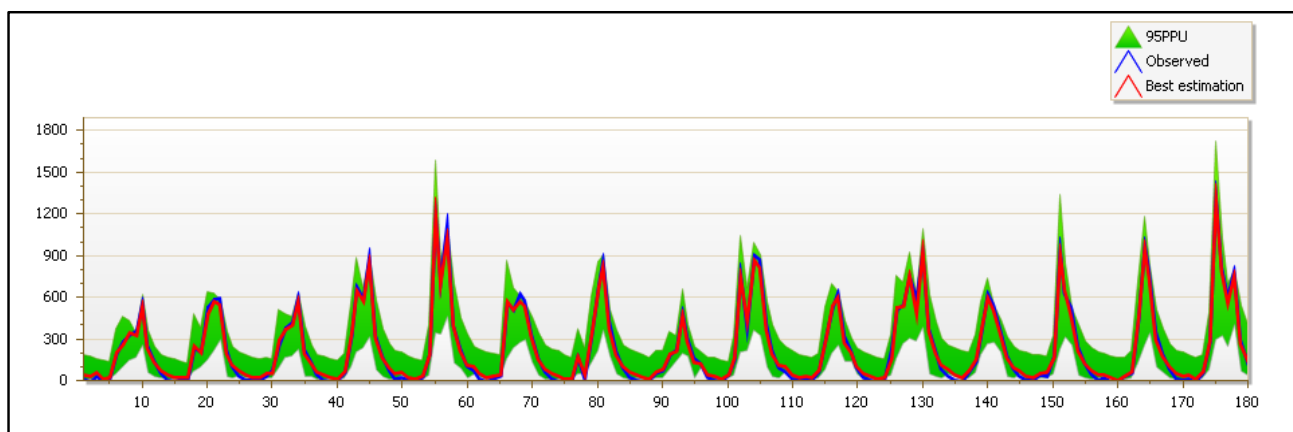


Figure 8. Comparison of measured and predicted monthly stream flow during the validation period (2018–2022).

4.7. Loss of Sediment Yield

Maximum soil loss from 2003 to 2022 occurred in sub-basin 15 (1432.052 metric tons/ha), followed by sub-basin 12 (1389.5295 metric tons/ha) and sub-basin 13 (1179.7055); while it was lowest in sub-basin 2 (248.12 metric tons/ha), followed by sub-basin 3 (305.387 metric tons/ha) and sub-basin 3 (341.0335 metric tons/ha).

Various studies state that rainfall is a major cause of soil loss. In one study, it was found that even though the discharge rate is different in summers and winters, soil loss is present in both conditions in the Skuterud catchment, southeast Norway [65]. In some cases, it was found that discharge plays an important role in the loss of soil. It has been observed that precipitation—in this case, rainfall—is a significant factor in soil loss from the area. Average soil loss from each sub-basin (refer to Table A3) was calculated to find the correlation between these two elements from 2003 to 2022. The year 2015 had the lowest rainfall, ranging from 5 mm to 8 mm in the post-monsoon months, which resulted in the least soil loss from the region. On the other hand, 2013 faced the maximum rainfall, thereby leading to maximum soil loss in the area. It can be observed that soil loss can be more related to precipitation than discharge. Both the graphs in Figure 9a follow a similar pattern, which is absent in Figure 9b. A strong correlation of 0.96 was observed between precipitation and soil loss, as compared to 0.91 between discharge and soil loss over the years. Due to a lack of data on other geographical factors, the relationship between them cannot be shown.

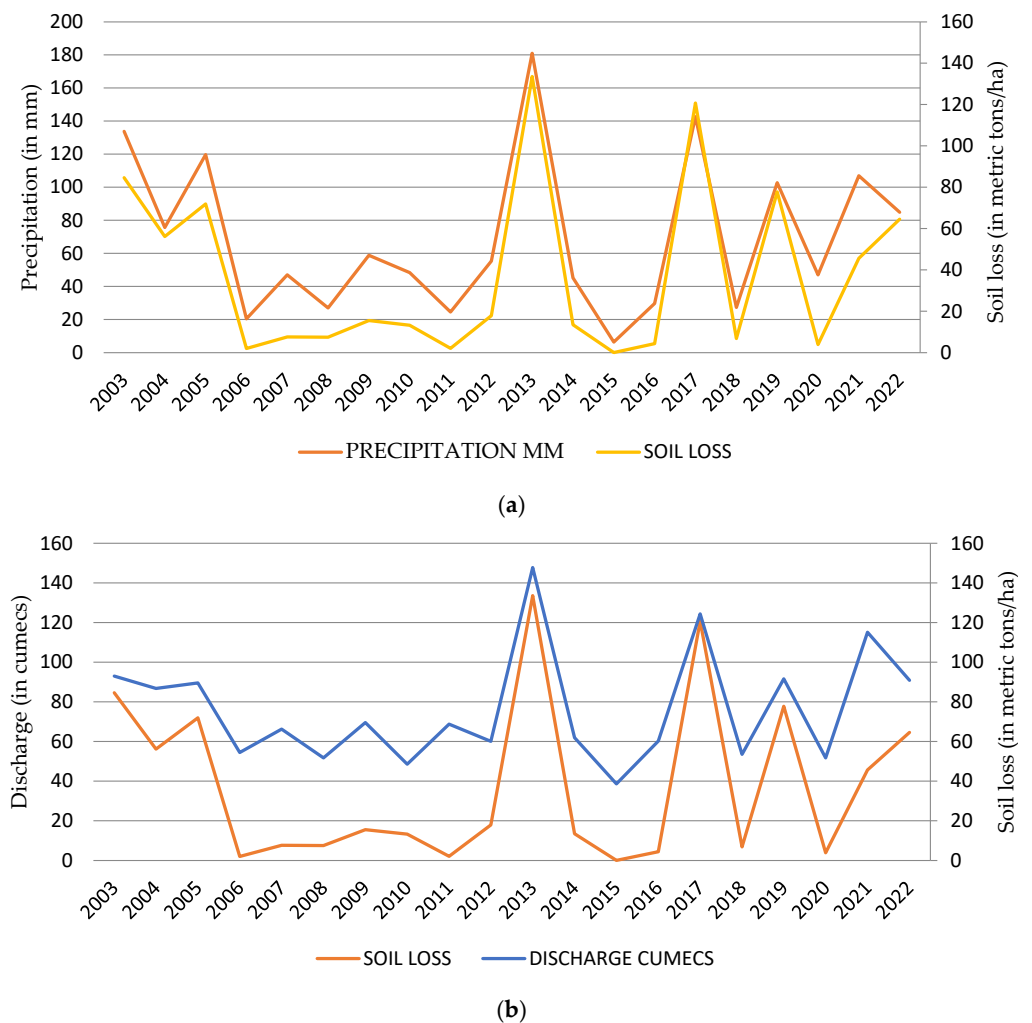


Figure 9. (a) Chart representing the relationship between rainfall and soil loss from 2003 to 2022. (b) Chart representing the relationship between discharge and soil loss from 2003 to 2022.

A thorough study of soil erosion patterns has also been carried out in various sub-basins within the study area, encompassing four distinct time periods: 2003–2007, 2007–2012, 2013–2017, and 2018–2022. Sub-basins have been categorized into four groups based on soil loss severity: very low (<5%), low (5% to 10%), high (10% to 15%), and high (>15%), as illustrated in Figure 10. The data in Table 4 show that the years between 2008 and 2012 experienced the lowest rates of soil erosion, a phenomenon potentially attributed to reduced precipitation levels during that period. Sub-basins 6, 16, 17, and 19 faced substantial soil loss during the years 2003–2007, 2013–2017, and 2018–2022, while sub-watersheds in regions 14 and 18 exhibited minimal soil loss. During 2003–2007, sub-basins 1, 5, 7, 8, 14, and 18 showcased the least soil loss, whereas sub-basins 6, 11, 16, 17, and 19 experienced the highest soil loss levels. It is worth noting that a definitive pattern of soil loss remains elusive in this region, owing to its high dependency on climatic variables. From 2013 to 2017, basins 2, 4, 6, 16, 17, and 19 witnessed the highest soil loss rates. All these basins throughout the years have faced a higher level of precipitation, leading to a higher discharge, and thereby higher soil loss. However, all basins registered lower erosion rates from 2018 to 2022. While multiple factors contribute to soil loss, a significant factor behind the reduced erosion during this period is diminished precipitation, indicating lower discharge levels. These combined factors collectively influenced the reduced soil erosion observed during this timeframe.

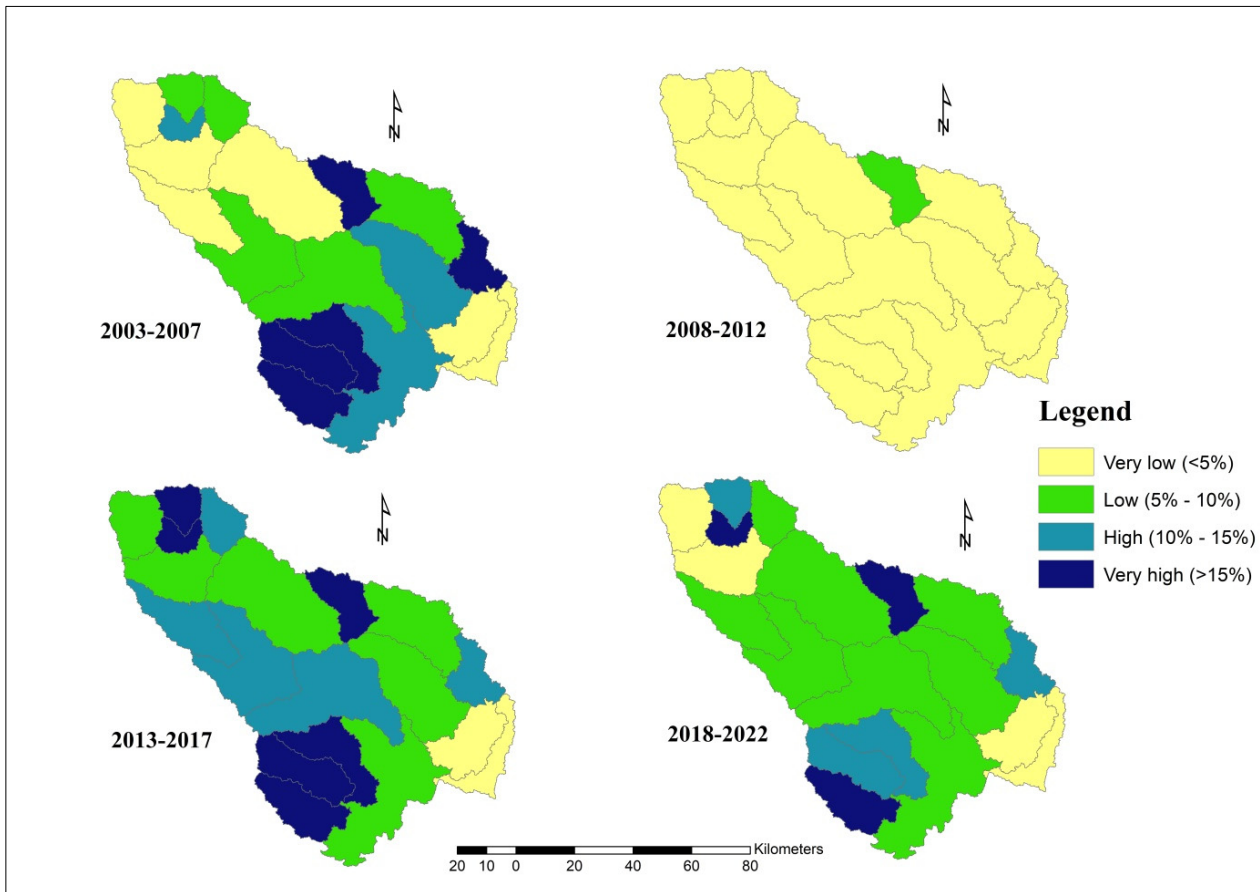


Figure 10. Soil loss from each sub-basin from 2003 to 2022.

Table 4. Soil loss calculation from each sub-basin.

Sub-Basin	Area (ha)	2003–2007		2008–2012		2013–2017		2018–2022	
		Soil loss (metric tons/ha)	% soil loss	Soil loss (metric tons/ha)	% soil loss	Soil loss (metric tons/ha)	% soil loss	Soil loss (metric tons/ha)	% soil loss
1	322.35	12.74	3.95	3.19	0.99	20.45	6.35	13.24	4.11
2	181.24	9.07	5.01	3.43	1.89	29.81	16.45	18.76	10.35
3	237.57	17.82	7.50	3.59	1.51	26.36	11.10	20.44	8.60
4	131.00	15.43	11.78	4.83	3.69	36.27	27.69	25.79	19.69
5	444.20	10.57	2.38	3.55	0.80	29.90	6.73	14.76	3.32
6	307.36	62.17	20.23	16.80	5.47	82.49	26.84	66.87	21.76
7	1023.80	47.42	4.63	12.71	1.24	70.35	6.87	53.22	5.20
8	443.94	21.34	4.81	6.90	1.55	63.52	14.31	25.32	5.70
9	589.00	41.19	6.99	9.15	1.55	35.40	6.01	31.45	5.34
10	688.45	63.86	9.28	16.86	2.45	84.18	12.23	59.65	8.66
11	264.43	51.33	19.41	13.12	4.96	37.47	14.17	36.21	13.69
12	948.48	77.32	8.15	19.92	2.10	108.96	11.49	71.71	7.56
13	721.82	83.24	11.53	22.77	3.15	66.05	9.15	63.88	8.85
14	395.55	12.08	3.05	2.99	0.76	8.35	2.11	9.69	2.45
15	928.48	104.56	11.26	25.98	2.80	85.40	9.20	70.46	7.59
16	404.65	61.80	15.27	12.70	3.14	75.07	18.55	49.73	12.29
17	394.41	64.99	16.48	15.43	3.91	94.37	23.93	55.13	13.98
18	236.67	11.51	4.86	3.14	1.33	8.84	3.73	7.92	3.35
19	376.03	76.06	20.23	16.26	4.32	71.06	18.90	60.38	16.06

5. Conclusions

The analysis of soil loss in various sub-basins from 2003 to 2022 reveals distinct patterns and factors influencing erosion dynamics. Sub-basin 15 emerged as the area with the highest soil loss, followed by sub-basins 12 and 13, while sub-basin 2 exhibited the lowest soil loss. Rainfall has been identified as a major driver of soil loss, with a strong correlation of 0.96 observed between precipitation and soil loss, compared to 0.91 for discharge and soil loss. A comprehensive examination of soil erosion patterns over four time periods highlighted the variability in soil loss severity across sub-basins. The years 2008 to 2012 experienced the lowest rates of soil erosion, potentially linked to reduced precipitation. Sub-basins 6, 16, 17, and 19 consistently faced substantial soil loss, while sub-basins 14 and 18 exhibited minimal erosion. Notably, a lack of definitive patterns in soil loss underscores the region's susceptibility to climatic variables. The reduced soil erosion observed from 2018 to 2022 is attributed to diminished precipitation, leading to lower discharge levels. These findings emphasize the complex interplay of climatic factors in influencing soil erosion dynamics.

This study encountered significant challenges, notably the prolonged processing time required by SWAT-CUP for data calibration. The absence of data from an ungauged station presented a critical limitation, compounded by a lack of field data to quantify sediment yield loss. The imperative goal for upcoming research is to delve deeper into the root causes of soil loss variations, facilitating the formulation of targeted conservation strategies crucial for safeguarding valuable soil resources amid evolving climate conditions.

Author Contributions: Conceptualization, A.M. and M.K.; methodology, A.M. and M.K.; software, A.M.; validation, A.M., M.K. and V.N.M.; formal analysis, A.M., M.K. and V.N.M.; investigation, A.M.; resources, M.K. and V.N.M.; data curation, A.M.; writing—original draft preparation, A.M.; writing—review and editing, M.K. and V.N.M.; visualization, A.M., M.K. and V.N.M.; supervision, M.K. All authors have read and agreed to the published version of the manuscript.

Funding: This research received no external funding.

Data Availability Statement: Data may be available on request.

Conflicts of Interest: The authors declare no conflict of interest.

Appendix A

Table A1. Confusion matrix for the accuracy assessment.

	Water	Forest	Agriculture	Barren	Urban
Water	9	0	0	1	0
Forest	0	39	9	0	0
Agriculture	0	3	40	1	0
Barren	0	0	2	41	0
Urban	0	1	0	0	10

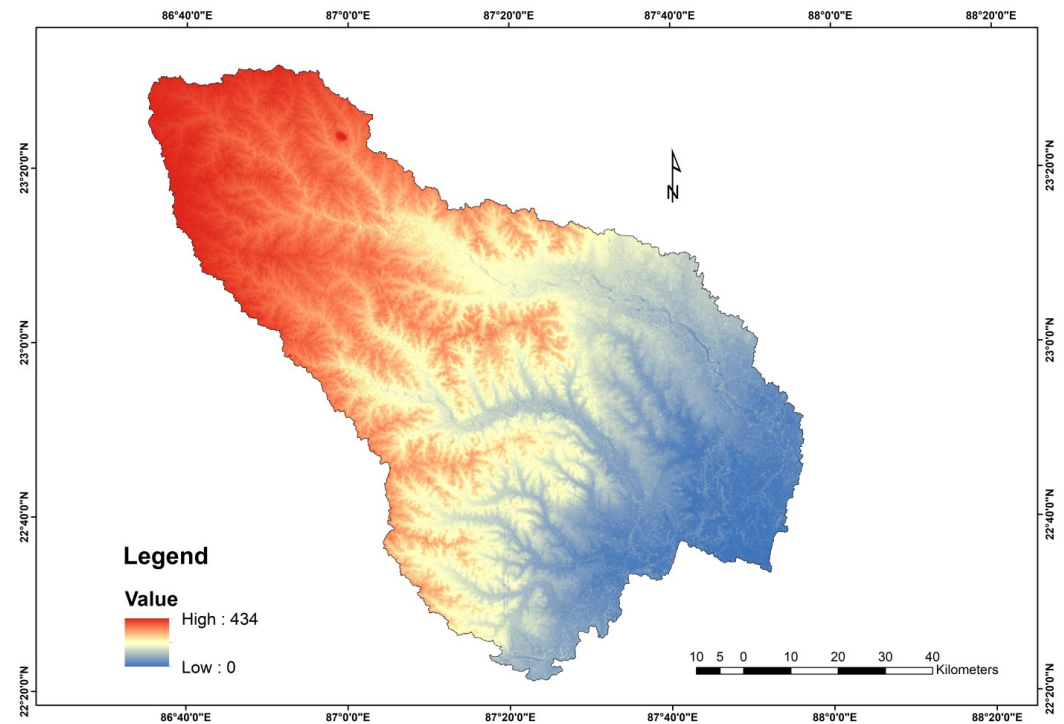


Figure A1. DEM of the study area.

Table A2. List of hydrological response units (HRUs).

Sl. No.	HRU No.	Sub-Basin 1	Area (sq. km)	% Watershed Area	% Sub-Basin Area
1	1	FRSD/Lf32-1b-3788/2-7	68.60	0.76	21.28
2	2	FRSD/Lf32-1b-3788/7-20	61.67	0.68	19.13
3	3	BARR/Lf32-1b-3788/7-20	82.65	0.91	25.64
4	4	BARR/Lf32-1b-3788/2-7	109.42	1.21	33.95
Sl. No.	HRU No.	Sub-Basin 2	Area (sq. km)	% Watershed Area	% Sub-Basin Area
1	5	FRSD/Lf32-1b-3788/2-7	34.16	0.38	18.85
2	6	FRSD/Lf32-1b-3788/7-20	33.83	0.37	18.67
3	7	BARR/Lf32-1b-3788/2-7	64.11	0.71	35.37
4	8	BARR/Lf32-1b-3788/7-20	49.13	0.54	27.11
Sl. No.	HRU No.	Sub-Basin 3	Area (sq. km)	% Watershed Area	% Sub-Basin Area
1	9	FRSD/Lf32-1b-3788/2-7	50.90	0.56	21.43
2	10	FRSD/Lf32-1b-3788/7-20	52.29	0.58	22.01
3	11	BARR/Lf32-1b-3788/2-7	42.21	0.47	17.77
4	12	BARR/Lf32-1b-3788/7-20	34.95	0.39	14.71
5	13	URHD/Lf32-1b-3788/7-20	26.58	0.29	11.19
6	14	URHD/Lf32-1b-3788/2-7	30.63	0.34	12.89
Sl. No.	HRU No.	Sub-Basin 4	Area (sq. km)	% Watershed Area	% Sub-Basin Area
1	15	FRSD/Lf32-1b-3788/7-20	22.23	0.25	16.97
2	16	FRSD/Lf32-1b-3788/2-7	20.37	0.23	15.55

Table A2. Cont.

Sl. No.	HRU No.	Sub-Basin 1	Area (sq. km)	% Watershed Area	% Sub-Basin Area
3	17	BARR/Lf32-1b-3788/2-7	34.57	0.38	26.39
4	18	BARR/Lf32-1b-3788/7-20	29.84	0.33	22.78
5	19	URHD/Lf32-1b-3788/2-7	12.51	0.14	9.55
6	20	URHD/Lf32-1b-3788/7-20	11.49	0.13	8.77
Sl. No.	HRU No.	Sub-Basin 5	Area (sq. km)	% Watershed Area	% Sub-Basin Area
1	21	FRSD/Lf32-1b-3788/2-7	117.64	1.30	26.48
2	22	FRSD/Lf32-1b-3788/7-20	126.52	1.40	28.48
3	23	BARR/Lf32-1b-3788/7-20	93.27	1.03	21.00
4	24	BARR/Lf32-1b-3788/2-7	106.77	1.18	24.04
Sl. No.	HRU No.	Sub-Basin 6	Area (sq. km)	% Watershed Area	% Sub-Basin Area
1	25	WATR/Be80-2a-3681/7-20	5.77	0.06	1.88
2	26	WATR/Be80-2a-3681/2-7	15.48	0.17	5.04
3	27	WATR/Be80-2a-3681/0-2	3.59	0.04	1.17
4	28	WATR/Lf96-2ab-6668/7-20	7.62	0.08	2.48
5	29	WATR/Lf96-2ab-6668/0-2	3.75	0.04	1.22
6	30	WATR/Lf96-2ab-6668/2-7	18.51	0.20	6.02
7	31	FRSD/Be80-2a-3681/7-20	18.39	0.20	5.98
8	32	FRSD/Be80-2a-3681/2-7	18.15	0.20	5.91
9	33	FRSD/Lf96-2ab-6668/7-20	38.44	0.43	12.51
10	34	FRSD/Lf96-2ab-6668/2-7	40.31	0.45	13.12
11	35	AGRC/Be80-2a-3681/2-7	14.71	0.16	4.79
12	36	AGRC/Be80-2a-3681/0-2	3.06	0.03	1.00
13	37	AGRC/Be80-2a-3681/7-20	5.48	0.06	1.78
14	38	AGRC/Lf96-2ab-6668/2-7	14.32	0.16	4.66
15	39	AGRC/Lf96-2ab-6668/0-2	3.43	0.04	1.12
16	40	AGRC/Lf96-2ab-6668/7-20	5.65	0.06	1.84
17	41	BARR/Be80-2a-3681/2-7	11.56	0.13	3.76
18	42	BARR/Be80-2a-3681/7-20	6.77	0.07	2.20
19	43	BARR/Be80-2a-3681/0-2	2.17	0.02	0.71
20	44	BARR/Lf96-2ab-6668/2-7	40.36	0.45	13.13
21	45	BARR/Lf96-2ab-6668/0-2	7.39	0.08	2.41
22	46	BARR/Lf96-2ab-6668/7-20	22.42	0.25	7.30
Sl. No.	HRU No.	Sub-Basin 7	Area (sq. km)	% Watershed Area	% Sub-Basin Area
1	46	FRSD/Lf10-2a-6665/7-20	34.00	0.38	3.32
2	47	FRSD/Lf10-2a-6665/2-7	40.50	0.45	3.96
3	48	FRSD/Lf32-1b-3788/7-20	152.98	1.69	14.94
4	49	FRSD/Lf32-1b-3788/2-7	153.08	1.69	14.95
5	50	FRSD/Lf96-2ab-6668/7-20	55.51	0.61	5.42
6	51	FRSD/Lf96-2ab-6668/2-7	57.40	0.64	5.61
7	52	BARR/Lf10-2a-6665/7-20	34.27	0.38	3.35
8	53	BARR/Lf10-2a-6665/0-2	13.76	0.15	1.34
9	54	BARR/Lf10-2a-6665/2-7	68.47	0.76	6.69
10	55	BARR/Lf32-1b-3788/2-7	164.14	1.82	16.03
11	56	BARR/Lf32-1b-3788/7-20	121.42	1.34	11.86
12	57	BARR/Lf96-2ab-6668/2-7	79.11	0.88	7.73
13	58	BARR/Lf96-2ab-6668/7-20	49.16	0.54	4.80
Sl. No.	HRU No.	Sub-Basin 8	Area (sq. km)	% Watershed Area	% Sub-Basin Area
1	58	FRSD/I-Ne-3729/2-7	58.14	0.64	13.10
2	59	FRSD/I-Ne-3729/7-20	73.17	0.81	16.48
3	60	FRSD/Lf32-1b-3788/7-20	59.82	0.66	13.47
4	61	FRSD/Lf32-1b-3788/2-7	50.10	0.55	11.28
5	62	BARR/I-Ne-3729/2-7	44.07	0.49	9.93
6	63	BARR/I-Ne-3729/7-20	41.94	0.46	9.45
7	64	BARR/Lf32-1b-3788/7-20	52.08	0.58	11.73
8	65	BARR/Lf32-1b-3788/2-7	64.63	0.72	14.56
Sl. No.	HRU No.	Sub-Basin 9	Area (sq. km)	% Watershed Area	% Sub-Basin Area
1	66	WATR/Be80-2a-3681/0-2	80.85	0.14	2.08
2	67	WATR/Be80-2a-3681/7-20	132.91	0.18	2.81
3	68	WATR/Be80-2a-3681/2-7	375.24	0.58	8.89

Table A2. Cont.

Sl. No.	HRU No.	Sub-Basin 1	Area (sq. km)	% Watershed Area	% Sub-Basin Area
4	69	FRSD/Be80-2a-3681/0-2	12.25	0.09	1.45
5	70	FRSD/Be80-2a-3681/7-20	16.58	0.26	4.01
6	71	FRSD/Be80-2a-3681/2-7	52.35	0.51	7.76
7	72	AGRC/Be80-2a-3681/2-7	8.55	2.16	33.20
8	73	AGRC/Be80-2a-3681/0-2	23.63	0.47	7.29
9	74	AGRC/Be80-2a-3681/7-20	45.73	0.69	10.57
10	75	BARR/Be80-2a-3681/7-20	195.56	0.34	5.17
11	76	BARR/Be80-2a-3681/2-7	42.93	0.90	13.86
12	77	BARR/Be80-2a-3681/0-2	62.26	0.19	2.91
Sl. No.	HRU No.	Sub-Basin 10	Area (sq. km)	% Watershed Area	% Sub-Basin Area
1	77	FRSD/Lf32-1b-3788/7-20	73.59	0.81	10.69
2	78	FRSD/Lf32-1b-3788/2-7	64.14	0.71	9.32
3	79	FRSD/Lf96-2ab-6668/7-20	92.82	1.03	13.48
4	80	FRSD/Lf96-2ab-6668/2-7	88.67	0.98	12.88
5	81	AGRC/Lf32-1b-3788/2-7	23.31	0.26	3.39
6	82	AGRC/Lf32-1b-3788/7-20	23.97	0.27	3.48
7	83	AGRC/Lf96-2ab-6668/7-20	30.72	0.34	4.46
8	84	AGRC/Lf96-2ab-6668/2-7	49.55	0.55	7.20
9	85	AGRC/Lf96-2ab-6668/0-2	9.50	0.11	1.38
10	86	BARR/Lf32-1b-3788/2-7	60.56	0.67	8.80
11	87	BARR/Lf32-1b-3788/7-20	46.31	0.51	6.73
12	88	BARR/Lf96-2ab-6668/2-7	68.10	0.75	9.89
13	89	BARR/Lf96-2ab-6668/7-20	44.50	0.49	6.46
14	90	BARR/Lf96-2ab-6668/0-2	12.71	0.14	1.85
Sl. No.	HRU No.	Sub-Basin 11	Area (sq. km)	% Watershed Area	% Sub-Basin Area
1	91	FRSD/Be80-2a-3681/0-2	6.24	0.07	2.36
2	92	FRSD/Be80-2a-3681/7-20	9.28	0.10	3.51
3	93	FRSD/Be80-2a-3681/2-7	27.76	0.31	10.50
4	94	AGRC/Be80-2a-3681/0-2	26.22	0.29	9.92
5	95	AGRC/Be80-2a-3681/2-7	85.84	0.95	32.46
6	96	AGRC/Je71-2a-3758/0-2	2.55	0.03	0.97
7	97	AGRC/Je71-2a-3758/7-20	1.67	0.02	0.63
8	98	AGRC/Je71-2a-3758/2-7	8.59	0.10	3.25
9	99	BARR/Be80-2a-3681/2-7	66.06	0.73	24.98
10	100	BARR/Be80-2a-3681/0-2	16.77	0.19	6.34
11	101	BARR/Be80-2a-3681/7-20	13.44	0.15	5.08
Sl. No.	HRU No.	Sub-Basin 12	Area (sq. km)	% Watershed Area	% Sub-Basin Area
1	102	FRSD/Be80-2a-3681/7-20	35.33	0.39	3.72
2	103	FRSD/Be80-2a-3681/2-7	49.92	0.55	5.26
3	104	FRSD/Lf96-2ab-6668/7-20	128.82	1.43	13.58
4	105	FRSD/Lf96-2ab-6668/2-7	155.94	1.73	16.44
5	106	AGRC/Be80-2a-3681/0-2	155.94	0.20	1.88
6	107	AGRC/Be80-2a-3681/2-7	17.88	0.75	7.17
7	108	AGRC/Be80-2a-3681/7-20	68.00	0.23	2.17
8	109	AGRC/Lf10-2a-6665/2-7	25.03	0.28	2.64
9	110	AGRC/Lf10-2a-6665/7-20	7.57	0.08	0.80
10	111	AGRC/Lf10-2a-6665/0-2	6.85	0.08	0.72
11	112	AGRC/Lf96-2ab-6668/7-20	39.27	0.43	4.14
12	113	AGRC/Lf96-2ab-6668/0-2	22.25	0.25	2.35
13	114	AGRC/Lf96-2ab-6668/2-7	98.24	1.09	10.36
14	115	BARR/Be80-2a-3681/2-7	54.13	0.60	5.71
15	116	BARR/Be80-2a-3681/0-2	13.31	0.15	1.40
16	117	BARR/Be80-2a-3681/7-20	16.26	0.18	1.71
17	118	BARR/Lf96-2ab-6668/2-7	116.67	1.29	12.30
18	119	BARR/Lf96-2ab-6668/7-20	47.04	0.52	4.96
19	120	BARR/Lf96-2ab-6668/0-2	25.33	0.28	2.67
Sl. No.	HRU No.	Sub-Basin 13	Area (sq. km)	% Watershed Area	% Sub-Basin Area
1	121	FRSD/Be80-2a-3681/7-20	28.20	0.31	3.91
2	122	FRSD/Be80-2a-3681/0-2	12.79	0.14	1.77
3	123	FRSD/Be80-2a-3681/2-7	60.74	0.67	8.42

Table A2. Cont.

Sl. No.	HRU No.	Sub-Basin 1	Area (sq. km)	% Watershed Area	% Sub-Basin Area
4	124	AGRC/Be80-2a-3681/0-2	81.77	0.90	11.33
5	125	AGRC/Be80-2a-3681/7-20	45.08	0.50	6.25
6	126	AGRC/Be80-2a-3681/2-7	280.02	3.10	38.79
7	127	AGRC/Lf10-2a-6665/2-7	62.03	0.69	8.59
8	128	AGRC/Lf10-2a-6665/7-20	15.03	0.10	2.08
9	129	AGRC/Lf10-2a-6665/0-2	15.28	0.17	2.12
10	130	BARR/Be80-2a-3681/7-20	15.54	0.17	2.15
11	131	BARR/Be80-2a-3681/2-7	70.59	0.78	9.78
12	132	BARR/Be80-2a-3681/0-2	18.64	0.21	2.58
13	133	BARR/Lf10-2a-6665/0-2	2.25	0.02	0.31
14	134	BARR/Lf10-2a-6665/2-7	10.36	0.11	1.44
15	135	BARR/Lf10-2a-6665/7-20	3.50	0.04	0.48
Sl. No.	HRU No.	Sub-Basin 14	Area (sq. km)	% Watershed Area	% Sub-Basin Area
1	136	FRSD/Be80-2a-3681/0-2	8.07	0.09	2.04
2	137	FRSD/Be80-2a-3681/2-7	31.69	0.35	8.01
3	138	FRSD/Be80-2a-3681/7-20	7.27	0.08	1.84
4	139	FRSD/Je71-2a-3758/7-20	3.29	0.04	0.83
5	140	FRSD/Je71-2a-3758/2-7	17.26	0.19	4.36
6	141	FRSD/Je71-2a-3758/0-2	4.69	0.05	1.19
7	142	AGRC/Be80-2a-3681/2-7	149.66	1.66	37.84
8	143	AGRC/Be80-2a-3681/0-2	56.87	0.63	14.38
9	144	AGRC/Je71-2a-3758/2-7	83.64	0.93	21.14
10	145	AGRC/Je71-2a-3758/0-2	33.11	0.37	8.37
Sl. No.	HRU No.	Sub-Basin 15	Area (sq. km)	% Watershed Area	% Sub-Basin Area
1	146	FRSD/Lf10-2a-6665/2-7	38.63	0.43	4.16
2	147	FRSD/Lf10-2a-6665/0-2	7.62	0.08	0.82
3	148	FRSD/Lf10-2a-6665/7-20	17.72	0.20	1.91
4	149	FRSD/Lf96-2ab-6668/2-7	23.58	0.26	2.54
5	150	FRSD/Lf96-2ab-6668/7-20	9.11	0.10	0.98
6	151	FRSD/Lf96-2ab-6668/0-2	5.29	0.06	0.57
7	152	FRSD/Lo49-2a-3808/7-20	7.27	0.08	0.78
8	153	FRSD/Lo49-2a-3808/2-7	23.79	0.26	2.56
9	154	FRSD/Lo49-2a-3808/0-2	5.43	0.06	0.58
10	155	AGRC/Lf32-1b-3788/2-7	299.32	3.31	32.24
11	156	AGRC/Lf10-2a-6665/0-2	96.13	1.06	10.35
12	157	AGRC/Lo49-2a-3808/7-20	26.44	0.29	2.85
13	158	AGRC/Lo49-2a-3808/0-2	56.22	0.62	6.06
14	159	AGRC/Lo49-2a-3808/2-7	174.05	1.93	18.75
15	160	BARR/Lf10-2a-6665/7-20	8.06	0.09	0.87
16	161	BARR/Lf10-2a-6665/2-7	39.65	0.44	4.27
17	162	BARR/Lf10-2a-6665/0-2	11.16	0.12	1.20
18	163	BARR/Lf96-2ab-6668/2-7	33.52	0.37	3.61
19	164	ARR/Lf96-2ab-6668/7-20	7.16	0.08	0.77
20	165	BARR/Lf96-2ab-6668/0-2	9.26	0.10	1.00
21	166	BARR/Lo49-2a-3808/7-20	3.40	0.04	0.37
22	167	BARR/Lo49-2a-3808/0-2	6.34	0.07	0.68
23	168	BARR/Lo49-2a-3808/2-7	19.34	0.21	2.08
Sl. No.	HRU No.	Sub-Basin 16	Area (sq. km)	% Watershed Area	% Sub-Basin Area
1	169	FRSD/Lf10-2a-6665/0-2	3.50	0.04	0.86
2	170	FRSD/Lf10-2a-6665/2-7	17.76	0.20	4.39
3	171	FRSD/Lf10-2a-6665/7-20	7.15	0.08	1.77
4	172	FRSD/Lf96-2ab-6668/7-20	49.01	0.54	12.11
5	173	FRSD/Lf96-2ab-6668/2-7	73.83	0.82	18.25
6	174	AGRC/Lf10-2a-6665/2-7	65.61	0.73	16.21
7	175	AGRC/Lf10-2a-6665/0-2	22.59	0.25	5.58
8	176	AGRC/Lf96-2ab-6668/2-7	45.95	0.51	11.35
9	177	AGRC/Lf96-2ab-6668/0-2	11.50	0.13	2.84
10	178	AGRC/Lf96-2ab-6668/7-20	13.74	0.15	3.40
11	179	BARR/Lf10-2a-6665/0-2	6.16	0.07	1.52

Table A2. Cont.

Sl. No.	HRU No.	Sub-Basin 1	Area (sq. km)	% Watershed Area	% Sub-Basin Area
12	180	BARR/Lf10-2a-6665/2-7	19.94	0.22	4.93
13	181	BARR/Lf10-2a-6665/7-20	3.12	0.03	0.77
14	182	BARR/Lf96-2ab-6668/0-2	9.67	0.11	2.39
15	183	BARR/Lf96-2ab-6668/7-20	13.99	0.15	3.46
16	184	BARR/Lf96-2ab-6668/2-7	41.14	0.46	10.17
Sl. No.	HRU No.	Sub-Basin 17	Area (sq. km)	% Watershed Area	% Sub-Basin Area
1	185	FRSD/Lf10-2a-6665/2-7	16.32	0.18	4.14
2	186	FRSD/Lf10-2a-6665/7-20	11.41	0.13	2.89
3	187	FRSD/Lf96-2ab-6668/2-7	92.63	1.02	23.49
4	188	FRSD/Lf96-2ab-6668/7-20	66.11	0.73	16.76
5	189	AGRC/Lf10-2a-6665/2-7	15.65	0.17	3.97
6	190	AGRC/Lf10-2a-6665/0-2	4.46	0.05	1.13
7	191	AGRC/Lf10-2a-6665/7-20	4.86	0.05	1.23
8	192	AGRC/Lf96-2ab-6668/2-7	48.87	0.54	12.39
9	193	AGRC/Lf96-2ab-6668/7-20	18.99	0.21	4.82
10	194	AGRC/Lf96-2ab-6668/0-2	11.11	0.12	2.82
11	195	BARR/Lf10-2a-6665/0-2	1.80	0.02	0.46
12	196	BARR/Lf10-2a-6665/2-7	7.66	0.08	1.94
13	197	BARR/Lf10-2a-6665/7-20	3.02	0.03	0.77
14	198	BARR/Lf96-2ab-6668/2-7	55.33	0.61	14.03
15	199	BARR/Lf96-2ab-6668/0-2	11.47	0.13	2.91
16	200	BARR/Lf96-2ab-6668/7-20	24.71	0.27	6.27
Sl. No.	HRU No.	Sub-Basin 18	Area (sq. km)	% Watershed Area	% Sub-Basin Area
1	201	FRSD/Be80-2a-3681/7-20	1.47	0.02	0.62
2	202	FRSD/Be80-2a-3681/2-7	8.94	0.10	3.78
3	203	FRSD/Be80-2a-3681/0-2	2.67	0.03	1.13
4	204	FRSD/Je71-2a-3758/7-20	5.78	0.06	2.44
5	205	FRSD/Je71-2a-3758/0-2	6.22	0.07	2.63
6	206	FRSD/Je71-2a-3758/2-7	22.66	0.25	9.58
7	207	AGRC/Be80-2a-3681/0-2	12.58	0.14	5.31
8	208	AGRC/Be80-2a-3681/2-7	27.01	0.30	11.41
9	209	AGRC/Je71-2a-3758/0-2	43.51	0.48	18.38
10	210	AGRC/Je71-2a-3758/2-7	105.83	1.17	44.72
Sl. No.	HRU No.	Sub-Basin 19	Area (sq. km)	% Watershed Area	% Sub-Basin Area
1	211	FRSD/Lf10-2a-6665/2-7	15.59	0.17	4.15
2	212	FRSD/Lf10-2a-6665/7-20	13.44	0.15	3.57
3	213	FRSD/Lf96-2ab-6668/2-7	101.21	1.12	26.91
4	214	FRSD/Lf96-2ab-6668/7-20	63.59	0.70	16.91
5	215	AGRC/Lf10-2a-6665/2-7	4.02	0.04	1.07
6	216	AGRC/Lf10-2a-6665/7-20	2.78	0.03	0.74
7	217	AGRC/Lf96-2ab-6668/2-7	38.23	0.42	10.17
8	218	AGRC/Lf96-2ab-6668/7-20	13.52	0.15	3.59
9	219	AGRC/Lf96-2ab-6668/0-2	8.58	0.09	2.28
10	220	BARR/Lf10-2a-6665/7-20	4.77	0.05	1.27
11	221	BARR/Lf10-2a-6665/2-7	7.35	0.08	1.96
12	222	BARR/Lf96-2ab-6668/0-2	13.69	0.15	3.64
13	223	BARR/Lf96-2ab-6668/2-7	63.00	0.70	16.75
14	224	BARR/Lf96-2ab-6668/7-20	26.28	0.29	6.99

Table A3. Average precipitation, discharge, and soil loss measured for each sub-basin for the post-monsoon season (October–November).

YEAR	2003	2004	2005	2006	2007	2008	2009	2010	2011	2012	2013	2014	2015	2016	2017	2018	2019	2020	2021	2022
Sub-Basin 1																				
PRECIPITATION (in mm)	119.65	55.85	89.50	16.85	28.10	14.15	56.20	38.20	26.30	53.65	171.70	46.90	5.60	18.55	138.95	20.65	86.35	43.65	106.80	90.50
DISCHARGE (in cumecs)	14.02	11.88	10.99	7.97	9.17	6.87	10.09	5.84	10.45	9.63	22.64	9.63	5.33	9.09	19.61	7.68	13.22	7.98	17.45	14.82
SOIL LOSS (metric tons/ha)	21.45	13.90	26.68	0.38	1.30	0.49	5.69	1.70	1.50	6.59	57.80	11.66	0.05	0.36	32.39	1.41	20.53	2.26	19.58	22.41
Sub-Basin 2																				
PRECIPITATION (in mm)	119.65	55.85	89.50	16.85	28.10	14.15	56.20	38.20	26.30	53.65	171.70	46.90	5.60	18.55	138.95	20.65	86.35	43.65	106.80	90.50
DISCHARGE (in cumecs)	7.84	6.60	6.14	4.37	5.03	3.77	5.59	3.22	5.74	5.33	12.62	5.34	2.92	4.99	10.93	4.23	7.33	4.40	9.56	8.24
SOIL LOSS (metric tons/ha)	18.48	10.15	14.61	0.57	1.56	0.46	6.97	2.17	1.36	6.20	92.01	8.55	0.06	0.89	47.54	2.39	23.41	2.71	20.96	44.35
Sub-Basin 3																				
PRECIPITATION (in mm)	119.65	55.85	89.50	16.85	28.10	14.15	56.20	38.20	26.30	53.65	171.70	46.90	5.60	18.55	138.95	20.65	86.35	43.65	106.80	90.50
DISCHARGE (in cumecs)	10.34	8.82	8.10	6.03	6.92	5.19	7.52	4.23	7.92	7.18	16.70	7.16	4.04	6.84	14.55	5.76	9.75	6.00	12.59	10.95
SOIL LOSS (metric tons/ha)	30.68	14.47	43.02	0.47	0.47	0.52	7.58	2.43	0.65	6.77	56.94	15.62	0.06	0.48	58.70	1.59	24.11	2.16	24.07	50.25
Sub-Basin 4																				
PRECIPITATION (in mm)	119.65	55.85	89.50	16.85	28.10	14.15	56.20	38.20	26.30	53.65	171.70	46.90	5.60	18.55	138.95	20.65	86.35	43.65	106.80	90.50
DISCHARGE (in cumecs)	27.40	23.09	21.46	15.33	17.64	13.22	19.58	11.19	20.16	18.67	44.23	18.68	10.23	17.49	38.29	14.82	25.68	15.43	33.66	28.84
SOIL LOSS (metric tons/ha)	32.11	14.48	28.18	0.64	1.74	0.50	6.96	2.76	1.22	12.69	105.87	9.40	0.06	0.54	65.50	2.93	38.84	1.82	22.95	62.40
Sub-Basin 5																				
PRECIPITATION (in mm)	119.65	55.85	89.50	16.85	28.10	14.15	56.20	38.20	26.30	53.65	171.70	46.90	5.60	18.55	138.95	20.65	86.35	43.65	106.80	90.50

Table A3. Cont.

YEAR	2003	2004	2005	2006	2007	2008	2009	2010	2011	2012	2013	2014	2015	2016	2017	2018	2019	2020	2021	2022
Sub-Basin 5																				
DISCHARGE (in cumecs)	47.43	40.55	37.20	27.77	31.88	23.90	34.56	20.15	36.27	33.05	76.45	32.98	18.64	31.59	66.52	26.57	45.02	27.53	59.35	50.42
SOIL LOSS (metric tons/ha)	32.11	7.40	11.43	0.60	1.30	0.57	5.80	1.42	1.39	8.57	59.21	10.00	0.03	0.70	79.57	1.41	26.60	2.95	26.24	16.57
Sub-Basin 6																				
PRECIPITATION (in mm)	121.65	69.15	119.65	19.00	43.60	26.20	56.50	42.90	22.60	57.05	170.90	42.75	5.45	20.20	144.05	20.05	86.60	39.95	106.60	93.45
DISCHARGE (in cumecs)	115.45	105.33	104.49	67.32	80.20	61.83	87.44	54.04	87.07	80.29	184.87	80.09	46.62	76.20	165.27	64.26	108.92	65.23	144.36	124.27
SOIL LOSS (metric tons/ha)	101.33	82.83	115.82	1.66	9.21	8.06	26.15	11.80	1.79	36.21	163.15	20.26	0.07	2.48	226.46	3.94	62.54	4.51	69.32	194.02
Sub-Basin 7																				
PRECIPITATION (in mm)	121.65	69.15	119.65	19.00	43.60	26.20	56.50	42.90	22.60	57.05	170.90	42.75	5.45	20.20	144.05	20.05	86.60	39.95	106.60	93.45
DISCHARGE (in cumecs)	102.17	92.35	90.86	59.59	70.68	54.28	76.99	47.26	77.11	71.06	163.77	70.86	41.08	67.47	145.86	56.80	96.44	57.86	127.94	109.81
SOIL LOSS (metric tons/ha)	75.31	56.37	93.85	1.32	10.26	8.74	17.82	7.20	2.10	27.71	132.57	15.58	0.09	2.19	201.30	4.56	93.54	4.64	55.57	107.80
Sub-Basin 8																				
PRECIPITATION (in mm)	119.65	55.85	89.50	16.85	28.10	14.15	56.20	38.20	26.30	53.65	171.70	46.90	5.60	18.55	138.95	20.65	86.35	43.65	106.80	90.50
DISCHARGE (in cumecs)	20.30	17.64	15.98	12.49	14.29	10.78	15.16	9.22	16.14	14.60	32.36	14.53	8.51	14.30	28.43	11.92	19.57	12.31	25.61	21.79
SOIL LOSS (metric tons/ha)	37.00	22.69	43.52	0.99	2.52	1.10	12.10	2.92	2.95	15.42	176.85	19.91	0.08	0.81	119.94	4.11	38.59	4.41	37.79	41.70
Sub-Basin 9																				
PRECIPITATION (in mm)	124.65	79.70	143.20	19.60	62.30	42.00	57.25	49.55	18.80	59.85	159.50	38.40	8.20	25.45	145.50	20.05	94.25	43.25	102.60	99.35
DISCHARGE (in cumecs)	138.63	128.68	132.89	78.74	98.03	76.77	105.80	66.72	102.52	95.22	221.10	93.88	55.80	89.55	199.64	75.87	131.53	77.60	173.95	149.43
SOIL LOSS (metric tons/ha)	78.74	58.96	56.99	1.10	10.18	9.18	12.59	8.93	0.50	14.58	60.53	6.03	0.05	2.05	108.37	1.28	62.15	1.67	34.64	57.50
Sub-Basin 10																				
PRECIPITATION (in mm)	143.85	82.75	126.55	22.00	47.40	25.30	60.65	53.10	26.40	54.90	195.95	48.60	5.60	35.85	141.35	33.95	110.00	50.45	106.60	80.20

Table A3. Cont.

YEAR	2003	2004	2005	2006	2007	2008	2009	2010	2011	2012	2013	2014	2015	2016	2017	2018	2019	2020	2021	2022
Sub-Basin 10																				
DISCHARGE (in cumecs)	55.88	51.59	51.59	34.42	39.88	30.33	41.61	29.73	42.87	36.19	88.99	38.57	23.86	37.51	71.65	33.80	55.28	31.76	67.97	53.29
SOIL LOSS (metric tons/ha)	108.82	68.40	128.54	3.63	9.91	6.90	22.64	22.57	4.05	28.17	227.86	18.11	0.06	8.74	166.12	14.55	118.56	6.49	73.95	84.68
Sub-Basin 11																				
PRECIPITATION (in mm)	147.20	94.05	144.35	23.85	67.50	41.40	61.30	57.90	22.50	56.30	185.60	42.05	8.20	41.70	147.30	33.10	123.20	51.05	108.45	76.40
DISCHARGE (in cumecs)	151.30	140.41	146.43	84.55	106.29	83.54	114.15	73.49	109.79	101.53	240.35	100.22	59.99	96.10	214.80	82.08	144.36	83.31	188.30	158.81
SOIL LOSS (metric tons/ha)	108.79	67.33	66.81	2.26	11.45	11.34	13.86	23.61	1.86	14.92	101.32	5.86	0.03	5.77	74.37	6.65	110.42	2.70	36.50	24.77
Sub-Basin 12																				
PRECIPITATION (in mm)	143.85	82.75	126.55	22.00	47.40	25.30	60.65	53.10	26.40	54.90	195.95	48.60	5.60	35.85	141.35	33.95	110.00	50.45	106.60	80.20
DISCHARGE (in cumecs)	104.07	97.15	99.69	62.94	73.29	55.89	76.60	56.46	77.92	64.73	166.71	70.28	43.70	67.84	129.95	62.76	103.30	57.51	126.10	95.14
SOIL LOSS (metric tons/ha)	152.00	100.25	118.57	4.70	11.05	10.95	27.48	28.19	2.88	30.10	293.55	29.61	0.07	10.78	210.79	15.92	110.56	6.08	89.14	136.84
Sub-Basin 13																				
PRECIPITATION (in mm)	147.20	94.05	144.35	23.85	67.50	41.40	61.30	57.90	22.50	56.30	185.60	42.05	8.20	41.70	147.30	33.10	123.20	51.05	108.45	76.40
DISCHARGE (in cumecs)	36.04	34.80	38.85	19.32	26.10	21.67	25.65	21.46	23.69	19.53	55.32	20.35	14.78	21.18	44.05	20.15	38.17	18.58	43.83	28.57
SOIL LOSS (metric tons/ha)	193.70	112.40	86.04	4.88	19.18	25.52	24.70	32.02	3.22	28.38	143.31	10.28	0.08	10.58	166.01	8.98	169.70	5.01	72.23	63.50
Sub-Basin 14																				
PRECIPITATION (in mm)	147.20	94.05	144.35	23.85	67.50	41.40	61.30	57.90	22.50	56.30	185.60	42.05	8.20	41.70	147.30	33.10	123.20	51.05	108.45	76.40
DISCHARGE (in cumecs)	207.45	195.30	207.05	116.20	148.55	118.45	155.05	107.86	148.35	132.60	327.40	132.83	84.29	130.25	284.00	114.56	204.80	113.21	258.90	204.15
SOIL LOSS (metric tons/ha)	33.00	17.18	7.76	0.54	1.92	2.23	3.04	5.95	0.12	3.59	23.29	1.82	0.00	1.82	14.83	0.64	18.48	0.16	16.33	12.81
Sub-Basin 15																				
PRECIPITATION (in mm)	147.20	94.05	144.35	23.85	67.50	41.40	61.30	57.90	22.50	56.30	185.60	42.05	8.20	41.70	147.30	33.10	123.20	51.05	108.45	76.40

Table A3. Cont.

YEAR	2003	2004	2005	2006	2007	2008	2009	2010	2011	2012	2013	2014	2015	2016	2017	2018	2019	2020	2021	2022
Sub-Basin 15																				
DISCHARGE (in cumecs)	213.40	203.75	213.40	130.14	155.45	121.36	159.35	123.49	159.65	130.50	338.00	142.13	93.38	140.00	264.50	130.49	217.45	118.80	260.60	190.10
SOIL LOSS (metric tons/ha)	194.01	134.31	167.00	4.32	23.17	30.37	27.56	38.36	5.20	28.43	206.37	12.51	0.16	10.96	197.02	18.87	170.22	7.59	75.80	79.82
Sub-Basin 16																				
PRECIPITATION (in mm)	143.85	82.75	126.55	22.00	47.40	25.30	60.65	53.10	26.40	54.90	195.95	48.60	5.60	35.85	141.35	33.95	110.00	50.45	106.60	80.20
DISCHARGE (in cumecs)	41.73	40.30	42.03	26.60	30.86	23.66	31.62	24.65	32.39	25.94	66.83	28.94	18.85	28.11	51.10	26.52	42.45	23.59	50.94	37.48
SOIL LOSS (metric tons/ha)	110.15	81.80	106.12	2.41	8.50	6.44	21.13	14.45	2.47	19.01	199.58	14.16	0.05	6.44	155.15	10.67	105.64	6.46	55.21	70.66
Sub-Basin 17																				
PRECIPITATION (in mm)	143.85	82.75	126.55	22.00	47.40	25.30	60.65	53.10	26.40	54.90	195.95	48.60	5.60	35.85	141.35	33.95	110.00	50.45	106.60	80.20
DISCHARGE (in cumecs)	20.61	19.88	20.73	13.11	15.22	11.65	15.59	12.15	15.95	12.79	32.95	14.24	9.25	13.86	25.20	13.03	20.92	11.60	25.11	18.48
SOIL LOSS (metric tons/ha)	121.65	84.42	107.23	3.18	8.46	7.52	24.13	20.23	2.55	22.70	229.15	21.89	0.07	8.65	212.07	13.33	122.77	5.17	64.16	70.23
Sub-Basin 18																				
PRECIPITATION (in mm)	147.20	94.05	144.35	23.85	67.50	41.40	61.30	57.90	22.50	56.30	185.60	42.05	8.20	41.70	147.30	33.10	123.20	51.05	108.45	76.40
DISCHARGE (in cumecs)	432.85	411.40	433.60	254.35	314.45	248.15	323.90	239.40	317.45	270.25	684.60	282.60	183.75	278.50	563.85	252.80	435.95	239.05	536.20	404.50
SOIL LOSS (metric tons/ha)	23.68	22.11	8.73	0.74	2.31	3.05	3.73	4.75	0.18	3.98	22.12	1.23	0.00	1.55	19.29	0.30	17.98	0.18	11.35	9.78
Sub-Basin 19																				
PRECIPITATION (in mm)	143.85	82.75	126.55	22.00	47.40	25.30	60.65	53.10	26.40	54.90	195.95	48.60	5.60	35.85	141.35	33.95	110.00	50.45	106.60	80.20
DISCHARGE (in cumecs)	19.64	18.84	19.68	12.34	14.34	10.97	14.74	11.47	14.98	12.07	31.32	13.43	8.66	13.06	23.92	12.25	19.81	10.91	23.77	17.50
SOIL LOSS (metric tons/ha)	133.63	97.78	135.16	3.76	9.94	8.22	24.48	19.78	2.96	25.83	186.41	23.21	0.04	7.30	138.36	15.75	142.06	6.63	61.03	76.40

References

1. Arshad, M.; Martin, S. Identifying critical limits for soil quality indicators in agro-ecosystems. *Agric. Ecosyst. Environ.* **2002**, *88*, 153–160. [[CrossRef](#)]
2. Nasir, M.J.; Ahmad, W.; Jun, C.; Iqbal, J.; Bateni, S.M. Soil erosion susceptibility assessment of Swat River sub-watersheds using the morphometry-based compound factor approach and GIS. *Environ. Earth Sci.* **2023**, *82*, 315. [[CrossRef](#)]
3. Pimentel, D. Soil Erosion: A Food and Environmental Threat. *Environ. Dev. Sustain.* **2006**, *8*, 119–137. [[CrossRef](#)]
4. Chalise, D.; Kumar, L.; Kristiansen, P. Land Degradation by Soil Erosion in Nepal: A Review. *Soil Syst.* **2019**, *3*, 12. [[CrossRef](#)]
5. Pandey, S.; Kumar, P.; Zlatic, M.; Nautiyal, R.; Panwar, V.P. Recent advances in assessment of soil erosion vulnerability in a watershed. *Int. Soil Water Conserv. Res.* **2021**, *9*, 305–318. [[CrossRef](#)]
6. Erenstein, O. *The Economics of Soil Conservation in Developing Countries: The Case of Crop Residue Mulching*; Wageningen University: Wageningen, The Netherlands, 1999.
7. Tibebe, D.; Bewket, W. Surface runoff and soil erosion estimation using the SWAT model in the Keleta Watershed, Ethiopia. *Land Degrad. Dev.* **2010**, *22*, 551–564. [[CrossRef](#)]
8. Mekonnen, Y.A.; Manderso, T.M. Land use/land cover change impact on streamflow using Arc-SWAT model, in case of Fetam watershed, Abbay Basin, Ethiopia. *Appl. Water Sci.* **2023**, *13*, 111. [[CrossRef](#)]
9. Wischmeier, W.H.; Smith, D.D. *Predicting Rainfall Erosion Losses: A Guide to Conservation Planning*; Department of Agriculture, Science and Education Administration: Washington, DC, USA, 1978.
10. Kaur, R.; Srinivasan, R.; Mishra, K.; Dutta, D.; Prasad, D.; Bansal, G. Assessment of a SWAT model for soil and water management in India. *Land Use Water Resour. Res.* **2003**, *3*, 1–7.
11. Merritt, W.; Letcher, R.; Jakeman, A. A review of erosion and sediment transport models. *Environ. Model. Softw.* **2003**, *18*, 761–799. [[CrossRef](#)]
12. Rawat, J.S.; Joshi, R.C.; Mesia, M. Estimation of erosivity index and soil loss under different land uses in the tropical foothills of Eastern Himalaya (India). *Trop. Ecol.* **2013**, *54*, 47–58.
13. Bryan, R.B. Soil erodibility and processes of water erosion on hillslope. *Geomorphology* **2000**, *32*, 385–415. [[CrossRef](#)]
14. Kouli, M.; Soupios, P.; Vallianatos, F. Soil erosion prediction using the Revised Universal Soil Loss Equation (RUSLE) in a GIS framework, Chania, Northwestern Crete, Greece. *Environ. Geol.* **2008**, *57*, 483–497. [[CrossRef](#)]
15. Lal, R. Soil degradation by erosion. *Land Degrad. Dev.* **2001**, *12*, 519–539. [[CrossRef](#)]
16. Morgan, R.P.C. *Soil Erosion and Conservation*, 3rd ed.; Blackwell: Malden, MA, USA, 2005.
17. Panda, C.; Das, D.M.; Raul, S.K.; Sahoo, B.C. Sediment yield prediction and prioritization of sub-watersheds in the Upper Subarnarekha basin (India) using SWAT. *Arab. J. Geosci.* **2021**, *14*, 809. [[CrossRef](#)]
18. Mosbahi, M.; Benabdallah, S.; Boussema, M.R. Assessment of soil erosion risk using SWAT model. *Arab. J. Geosci.* **2012**, *6*, 4011–4019. [[CrossRef](#)]
19. Phuong, T.T.; Shrestha, R.P.; Chuong, H.V. Simulation of Soil Erosion Risk in the Upstream Area of Bo River Watershed. In *Redefining Diversity & Dynamics of Natural Resources Management in Asia*; Elsevier: Amsterdam, The Netherlands, 2017; Volume 3, pp. 87–99. [[CrossRef](#)]
20. İrvem, A.; Topaloğlu, F.; Uygur, V. Estimating spatial distribution of soil loss over Seyhan River Basin in Turkey. *J. Hydrol.* **2007**, *336*, 30–37. [[CrossRef](#)]
21. Terranova, O.; Antronico, L.; Coscarelli, R.; Iaquina, P. Soil erosion risk scenarios in the Mediterranean environment using RUSLE and GIS: An application model for Calabria (southern Italy). *Geomorphology* **2009**, *112*, 228–245. [[CrossRef](#)]
22. Demirci, A.; Karaburun, A. Estimation of soil erosion using RUSLE in a GIS framework: A case study in the Buyukcekmece Lake watershed, northwest Turkey. *Environ. Earth Sci.* **2011**, *66*, 903–913. [[CrossRef](#)]
23. Ganasri, B.P.; Ramesh, H. Assessment of soil erosion by RUSLE model using remote sensing and GIS—A case study of Nethravathi Basin. *Geosci. Front.* **2016**, *7*, 953–961. [[CrossRef](#)]
24. Pal, S.C.; Chakraborty, R. Modeling of water induced surface soil erosion and the potential risk zone prediction in a sub-tropical watershed of Eastern India. *Model. Earth Syst. Environ.* **2018**, *5*, 369–393. [[CrossRef](#)]
25. Williams, J.R. Sediment-Yield Prediction with Universal Equation Using Runoff Energy Factor. In *Present and Prospective Technology for Predicting Sediment Yield and Sources*; US Department of Agriculture, Agriculture Research Service: Washington, DC, USA, 1975; Volume 40.
26. Beasley, D.B.; Huggins, L.F.; Monke, E.J. ANSWERS: A Model for Watershed Planning. *Trans. ASAE* **1980**, *23*, 0938–0944. [[CrossRef](#)]
27. Young, R.A. AGNPS: A Non-Point-Source Pollution Model for Evaluating Agricultural Watersheds. *J. Soil Water Conserv.* **1989**, *44*, 168–173.
28. Abbott, M.; Bathurst, J.; Cunge, J.; O’Connell, P.; Rasmussen, J. An introduction to the European Hydrological System—Système Hydrologique Européen, “SHE”, 1: History and philosophy of a physically-based, distributed modelling system. *J. Hydrol.* **1986**, *87*, 45–59. [[CrossRef](#)]
29. Ewen, J.; Parkin, G.; O’Connell, P.E. SHETRAN: Distributed River Basin Flow and Transport Modeling System. *J. Hydrol. Eng.* **2000**, *5*, 250–258. [[CrossRef](#)]
30. Birkinshaw, S.J.; James, P.; Ewen, J. Graphical user interface for rapid set-up of SHETRAN physically-based river catchment model. *Environ. Model. Softw.* **2010**, *25*, 609–610. [[CrossRef](#)]

31. Schulze, R.E. Hydrology and Agrohydrology: A Text to Accompany the ACRU 3.00 Agrohydrological Modelling System. In *South Africa Water Research Commission Report, TT 95/69*; Dept. of Agricultural Engineering, University of Natal: Pietermaritzburg, South Africa, 1995.
32. Arnold, J.G.; Srinivasan, R.; Muttiah, R.S.; Williams, J.R. Large area hydrologic modeling and assessment Part I: Model development. *JAWRA J. Am. Water Resour. Assoc.* **1998**, *34*, 73–89. [[CrossRef](#)]
33. Williams, J.R.; Arnold, J.G.; Kiniry, J.R.; Gassman, P.W.; Green, C.H. History of model development at Temple, Texas. *Hydrol. Sci. J.* **2008**, *53*, 948–960. [[CrossRef](#)]
34. Gassman, P.W.; Reyes, M.R.; Green, C.H.; Arnold, J.G. The Soil and Water Assessment Tool: Historical Development, Applications, and Future Research Directions. *Trans. ASABE* **2007**, *50*, 1211–1250. [[CrossRef](#)]
35. Arnold, J.G.; Moriasi, D.N.; Gassman, P.W.; Abbaspour, K.C.; White, M.J.; Srinivasan, R.; Santhi, C.; Harmel, R.D.; van Griensven, A.; Van Liew, M.W.; et al. SWAT: Model Use, Calibration, and Validation. *Trans. ASABE* **2012**, *55*, 1491–1508. [[CrossRef](#)]
36. Gassman, P.W.; Sadeghi, A.M.; Srinivasan, R. Applications of the SWAT Model Special Section: Overview and Insights. *J. Environ. Qual.* **2014**, *43*, 1–8. [[CrossRef](#)]
37. Devia, G.K.; Ganasri, B.; Dwarakish, G. A Review on Hydrological Models. *Aquat. Procedia* **2015**, *4*, 1001–1007. [[CrossRef](#)]
38. Abbaspour, K.C.; Yang, J.; Maximov, I.; Siber, R.; Bogner, K.; Mieleitner, J.; Zobrist, J.; Srinivasan, R. Modelling hydrology and water quality in the pre-alpine/alpine Thur watershed using SWAT. *J. Hydrol.* **2007**, *333*, 413–430. [[CrossRef](#)]
39. Malik, S.; Pal, S.C. Potential flood frequency analysis and susceptibility mapping using CMIP5 of MIROC5 and HEC-RAS model: A case study of lower Dwarkeswar River, Eastern India. *SN Appl. Sci.* **2021**, *3*, 31. [[CrossRef](#)]
40. Inland River Ports. *Inland Waterway Transport*; Inland River Ports: St. Louis, MO, USA, 2016; pp. 141–157. [[CrossRef](#)]
41. Shit, P.K.; Maiti, R. Rill Hydraulics—An Experimental Study on Gully Basin in Lateritic Upland of Paschim Medinipur, West Bengal, India. *J. Geogr. Geol.* **2012**, *4*, 1. [[CrossRef](#)]
42. Bera, B.; Saha, S.; Bhattacharjee, S. Forest cover dynamics (1998 to 2019) and prediction of deforestation probability using binary logistic regression (BLR) model of Silabati watershed, India. *Trees For. People* **2020**, *2*, 100034. [[CrossRef](#)]
43. Mahala, A. Processes and Status of Land Degradation in a Plateau Fringe Region of Tropical Environment. *Environ. Process.* **2017**, *4*, 663–682. [[CrossRef](#)]
44. Nag, S.K.; Lahiri, A. Hydrochemical Characteristics of Groundwater for Domestic and Irrigation Purposes in Dwarakeswar Watershed Area, India. *Am. J. Clim. Chang.* **2012**, *1*, 217–230. [[CrossRef](#)]
45. Saraf, A.K.; Choudhury, P.R.; Roy, B.; Sarma, B.; Vijay, S.; Choudhury, S. GIS based surface hydrological modelling in identification of groundwater recharge zones. *Int. J. Remote. Sens.* **2004**, *25*, 5759–5770. [[CrossRef](#)]
46. Cervantes, J.; Garcia-Lamont, F.; Rodríguez-Mazahua, L.; Lopez, A. A comprehensive survey on support vector machine classification: Applications, challenges and trends. *Neurocomputing* **2019**, *408*, 189–215. [[CrossRef](#)]
47. Halder, S.; Das, S.; Basu, S. Use of support vector machine and cellular automata methods to evaluate impact of irrigation project on LULC. *Environ. Monit. Assess.* **2022**, *195*, 3. [[CrossRef](#)] [[PubMed](#)]
48. Zhang, Y. Support Vector Machine Classification Algorithm and Its Application. In *Information Computing and Applications: Third International Conference, ICICA 2012, Chengde, China, 14–16 September 2012. Proceedings, Part II 3*; Springer: Berlin/Heidelberg, Germany, 2012; pp. 179–186. [[CrossRef](#)]
49. Krause, P.; Boyle, D.P.; Båse, F. Comparison of different efficiency criteria for hydrological model assessment. *Adv. Geosci.* **2005**, *5*, 89–97. [[CrossRef](#)]
50. Nash, J.E.; Sutcliffe, J.V. River flow forecasting through conceptual models part I—A discussion of principles. *J. Hydrol.* **1970**, *10*, 282–290. [[CrossRef](#)]
51. Gupta, H.V.; Sorooshian, S.; Yapo, P.O. Status of Automatic Calibration for Hydrologic Models: Comparison with Multilevel Expert Calibration. *J. Hydrol. Eng.* **1999**, *4*, 135–143. [[CrossRef](#)]
52. Das, B.; Jain, S.; Singh, S.; Thakur, P. Evaluation of multisite performance of SWAT model in the Gomti River Basin, India. *Appl. Water Sci.* **2019**, *9*, 134. [[CrossRef](#)]
53. Moriasi, D.N.; Arnold, J.G.; van Liew, M.W.; Bingner, R.L.; Harmel, R.D.; Veith, T.L. Model evaluation guidelines for systematic quantification of accuracy in watershed simulations. *Trans. ASABE* **2007**, *50*, 885–900. [[CrossRef](#)]
54. Abbaspour, K.C.; Rouholahnejad, E.; Vaghefi, S.; Srinivasan, R.; Yang, H.; Kløve, B. A continental-scale hydrology and water quality model for Europe: Calibration and uncertainty of a high-resolution large-scale SWAT model. *J. Hydrol.* **2015**, *524*, 733–752. [[CrossRef](#)]
55. Abbaspour, K.C.; Johnson, C.A.; van Genuchten, M.T. Estimating Uncertain Flow and Transport Parameters Using a Sequential Uncertainty Fitting Procedure. *Vadose Zone J.* **2004**, *3*, 1340–1352. [[CrossRef](#)]
56. Yang, J.; Reichert, P.; Abbaspour, K.C.; Xia, J.; Yang, H. Comparing uncertainty analysis techniques for a SWAT application to the Chaohe Basin in China. *J. Hydrol.* **2008**, *358*, 1–23. [[CrossRef](#)]
57. Aown, A.; Kar, N.S. Lateritic Badland of Sinhati, Bankura, West Bengal: A Geomorphic Investigation. In *Neo-Thinking on Ganges-Brahmaputra Basin Geomorphology*; Springer: Berlin/Heidelberg, Germany, 2016; pp. 19–31. [[CrossRef](#)]
58. Shit, P.K.; Bhunia, G.S.; Maiti, R. Farmers’ Perceptions of Soil Erosion and Management Strategies in South Bengal in India. *Eur. J. Geogr.* **2015**, *6*, 85–100.
59. David, S.R.; Murphy, B.P.; Czuba, J.A.; Ahammad, M.; Belmont, P. USUAL Watershed Tools: A new geospatial toolkit for hydro-geomorphic delineation. *Environ. Model. Softw.* **2023**, *159*, 105576. [[CrossRef](#)]

60. Narsimlu, B.; Gosain, A.K.; Chahar, B.R. Assessment of Future Climate Change Impacts on Water Resources of Upper Sind River Basin, India Using SWAT Model. *Water Resour. Manag.* **2013**, *27*, 3647–3662. [[CrossRef](#)]
61. Narsimlu, B.; Gosain, A.K.; Chahar, B.R.; Singh, S.K.; Srivastava, P.K. SWAT Model Calibration and Uncertainty Analysis for Streamflow Prediction in the Kunwari River Basin, India, Using Sequential Uncertainty Fitting. *Environ. Process.* **2015**, *2*, 79–95. [[CrossRef](#)]
62. Suryavanshi, S.; Pandey, A.; Chaube, U.C. Hydrological Simulation of the Betwa River Basin (India) Using the SWAT Model. *Hydrol. Sci. J.* **2017**, *62*, 960–978. [[CrossRef](#)]
63. Khatun, S.; Sahana, M.; Jain, S.K.; Jain, N. Simulation of surface runoff using semi distributed hydrological model for a part of Satluj Basin: Parameterization and global sensitivity analysis using SWAT CUP. *Model. Earth Syst. Environ.* **2018**, *4*, 1111–1124. [[CrossRef](#)]
64. James, L.D.; Burges, S.J. Selection, Calibration, and Testing of Hydrologic Models. In *Hydrologic Modeling of Small Watersheds*; Haan, C.T., Johnson, H.P., Brakensiek, D.L., Eds.; ASAE Monograph; ASAE: St. Joseph, MI, USA, 1982; pp. 437–472.
65. Kværnø, S.H.; Stolte, J. Effects of soil physical data sources on discharge and soil loss simulated by the LISEM model. *Catena* **2012**, *97*, 137–149. [[CrossRef](#)]

Disclaimer/Publisher’s Note: The statements, opinions and data contained in all publications are solely those of the individual author(s) and contributor(s) and not of MDPI and/or the editor(s). MDPI and/or the editor(s) disclaim responsibility for any injury to people or property resulting from any ideas, methods, instructions or products referred to in the content.